Chemical Science

PERSPECTIVE

View Article Online
View Journal | View Issue

Cite this: *Chem. Sci.*, 2026, **17**, 6261

All publication charges for this article have been paid for by the Royal Society of Chemistry

# Microenvironment regulation in nanomaterial synthesis

Shuyi Pang,[a] Yuanduo Li,[a] Wenxia Xu,[a] Hangkai Shi,[a] Hongdong Li,[a] Jingqi Chi,[b] Jianping Lai *[a] and Lei Wang *[a]

Received 30th October 2025
Accepted 22nd February 2026

DOI: 10.1039/d5sc08395h

rsc.li/chemical-science

The controllable synthesis of nanomaterials serves as the core driving force for the development of energy, catalysis, biomedicine and other fields. Their performance depends on microstructures including size and morphology, whose formation is precisely regulated by the synthetic microenvironment. Traditional macroscale and extensive synthesis suffers from issues such as inhomogeneous mixing and uncontrollable mass and heat transfer, leading to non-uniform product structures that impede the precise construction of complex architectures. As an innovative preparation concept fundamentally distinct from traditional synthesis, synthetic microenvironment engineering features the core advantage of replacing macroscale rough operations with microscale precise regulation. *Via* three core dimensions—local physicochemical environment, spatial confinement effect, and external energy environment—it precisely manipulates the nucleation and growth processes, addressing the bottlenecks of conventional synthesis. Strategies across the three dimensions share the commonality of microscale regulation while possessing unique differentiated advantages; they can also be synergistically coupled to achieve controllable preparation of complex nanomaterials with uniform sizes and unique morphologies. This review focuses on microenvironment engineering strategies in nanomaterial synthesis, systematically summarizes the research progress of the three dimensions, compares the similarities and differences among various strategies, discusses their applications in hierarchical structure construction, crystal phase selection and surface modification, and analyzes the key challenges and future directions in fundamental research and industrial translation. It aims to provide a reference for the rational design, green synthesis and large-scale preparation of high-performance nanomaterials.

## 1 Introduction

In recent years, nanomaterials, serving as the core fundamental materials in modern high-tech industries, have shown extensive application prospects in numerous cutting-edge scientific and technological fields, including energy storage, catalytic conversion, biomedicine, and information devices, owing to their distinctive physical and chemical properties.[1–3] In the realm of energy storage, nanostructured electrode materials can remarkably enhance the energy density and cycle stability of lithium-ion batteries and supercapacitors. This offers novel avenues for the realization of efficient electrical energy storage.[4,5] Regarding catalytic conversion, nano-catalysts can enhance the efficiency of catalytic water splitting and the degradation ability of organic pollutants through the precise regulation of active sites and electronic structures. This, in turn, promotes the advancement of green chemistry.[6–8] In the field of biomedicine, functionalized nanoparticles are applicable to targeted drug delivery, tumor imaging, and high-efficiency treatment. They break through the biological barriers and selectivity limitations of traditional therapeutic methods.[9,10] Furthermore, in information devices, carbon nanotubes and two-dimensional materials provide the crucial material foundation for constructing high-mobility transistors, flexible electronic devices, and novel storage units. They contribute to the development of next-generation low-power and high-performance computing technologies.[11,12] However, these remarkable application prospects essentially depend on the precise and controllable preparation of nanomaterials. The key challenge in promoting the transition of nanomaterials from laboratory research to wide-ranging applications lies in how to precisely control their microstructures. This has also shifted the research focus towards a profound understanding and innovation of their synthesis processes.[13–15]

The properties of functional nanomaterials are highly coupled with the microstructure formed during their synthesis. Bridging the gap from microscopically controllable structures

---

[a] *Key Laboratory Base of Eco-Chemical Engineering, Ministry of Education, International Science and Technology Cooperation Base of Eco-Chemical Engineering and Green Manufacturing, College of Chemistry and Molecular Engineering, Qingdao University of Science and Technology, Qingdao 266042, P. R. China. E-mail: jplai@qust.edu.cn; inorchemwl@126.com*

[b] *College of Chemical Engineering, Qingdao University of Science and Technology, Qingdao 266042, P. R. China*

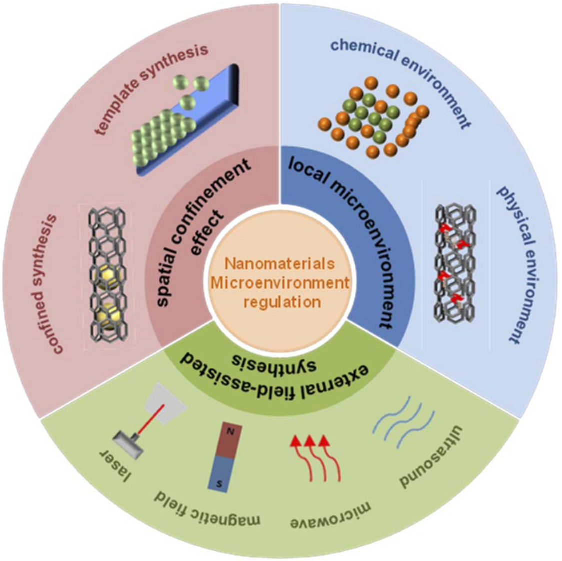

Fig. 1 Common nanomaterial microenvironmental control strategies.

to macroscopically applicable materials is the key to promoting their industrial applications.[16–24] In this context, synthetic microenvironment engineering, a novel preparation paradigm fundamentally different from traditional macroscopic synthetic strategies, is regarded as a central and effective approach to overcoming the above bottlenecks. Traditional synthesis mostly focuses on global, extensive parameter regulation of the reaction system, whereas synthetic microenvironment engineering takes the microscale reaction field as the core. Through precise design and dynamic control of local reaction conditions, it directionally guides precursor transformation, atomic nucleation, and crystal growth. The so-called synthetic microenvironment is a complex system covering three core dimensions: local physicochemical environment, spatial confinement effect, and external energy field (Fig. 1).[25–27] Key factors including reactant concentration, interfacial guidance of ligands/templates, and energy input from external fields all fall within these three dimensions. These factors are mutually coupled and collectively govern the transformation pathway of precursors, nucleation rate, crystal growth orientation, and the assembly behavior of the final materials. Strategies for microenvironment regulation in nanomaterial synthesis include local physical and chemical control (*e.g.*, local concentration, temperature, specific solvents, and ligand regulation), soft/hard templates and their synergistic strategies under spatial confinement, as well as external field-assisted approaches such as microwave, laser, magnetic field, and ultrasound.[28,29] All these are concrete implementations of the three core dimensions. Their unifying core lies in achieving precise microscale regulation to alter the thermodynamic and kinetic conditions of local reactions. This enables fine control over material properties such as size distribution, exposed crystal facets, porous structure, and even surface chemical states, thereby directionally optimizing the optical, electrical, catalytic, and mechanical performances of the materials.[30–36]

It is worth emphasizing that the regulation of synthetic microenvironments is essentially a multiscale, cross-process systematic engineering approach. The regulatory roles of the three core dimensions exhibit distinct characteristics and coupling effects at different scales.[37] At the molecular scale, the regulation of the local physicochemical environment plays a dominant role. The mass transfer and diffusion of reactants within confined spaces, as well as their interfacial interactions with templates and ligands, directly determine the uniformity and stability of initial nucleation.[38–40] At the nanoscale, spatial confinement and the local physicochemical environment act synergistically. The local pH gradient, ionic strength, and temperature field distribution during crystal growth, combined with the physical constraints of confined spaces, profoundly influence the final morphology and preferential exposure of crystal facets.[41–44] At the mesoscopic and even macroscopic scales, the external energy environment becomes a key regulatory tool. The introduction of external fields such as electric, magnetic, and acoustic fields enables non-contact control over reaction pathways and provides additional driving forces for material assembly. Together with the two aforementioned factors, they form synthetic technologies with distinctive advantages.[45,46] Such cross-scale correlations from molecular to macroscopic levels render synthetic microenvironment regulation not only a matter of local chemical behavior but also a field involving complex physical processes including energy and mass transport and phase interface evolution. Its elucidation urgently requires interdisciplinary approaches integrating materials science, chemistry, physics, and engineering.[47,48]

In recent years, with the rapid development of soft and hard templating, microreactor technology, external field-assisted synthesis, and biomimetic synthesis strategies, synthetic microenvironment regulation has gradually evolved from early phenomenological observation and empirical exploration to a stage of rational and systematic design.[49–52] For example, soft templates formed by the self-assembly of amphiphilic molecules can precisely guide the construction of ordered mesoporous materials; the introduction of external fields enables real-time and spatially resolved control over the synthesis process; and special solvents such as molten salts and liquid metals provide novel platforms for the design of microscale physicochemical environments.[53,54] The introduction of external fields can achieve real-time and spatially resolved control of the synthesis process, providing a brand-new path for customizing material structures.[55–57] In this process, the integration of advanced characterization techniques and computational simulation methods is playing an increasingly crucial role. Dynamic characterization methods such as *in situ* electron microscopy and synchrotron radiation X-ray absorption spectroscopy enable researchers to capture the evolution trajectory of material structures under the influence of the microenvironment in real space and energy space.[58–60] The combination of first-principles calculations, molecular dynamics simulations, and reaction–transport models further provides a theoretical framework and predictive tools for revealing the structure–activity relationships between microenvironmental parameters and material synthesis.[61,62] The establishment of this "characterization–simulation–design" research model is an important scientific foundation for the precise manufacturing of nanomaterials.

Despite remarkable achievements in the field of synthetic microenvironment regulation, numerous core challenges remain. First, the dynamic coupling mechanism and synergistic rules of the three core dimensions in complex heterogeneous and multicomponent systems are not yet fully understood. Second, the common and distinct features of various microenvironment regulation strategies lack systematic analysis, and the potential of cross-dimensional synergistic regulation has not been fully exploited. Third, the precise regulation strategies at the laboratory scale are difficult to translate into large-scale manufacturing, with obvious scale-up effects.[63,64] Against this background, this review focuses on the three core regulatory dimensions of synthetic microenvironments: local physicochemical environment, spatial confinement effect, and external energy environment.[65–69] We systematically summarize the recent research progress of typical regulation strategies under each dimension, with emphasis on analyzing their working mechanisms and applicable scenarios, and comparing their common characteristics and differential advantages. We also discuss the feasible pathways for cross-dimensional synergistic regulation and analyze the potential bottlenecks and future directions in industrial applications. This review aims to provide comprehensive references and insights for the rational design, green synthesis, and scalable preparation of high-performance nanomaterials.

## 2 Local microenvironment

The local physicochemical environment is one of the core dimensions for microenvironment regulation in nanomaterial synthesis. By precisely tailoring the physical and chemical conditions in microreaction zones, it enables directional guidance over the entire nucleation and growth process of materials, showing highly efficient and precise controllability. This dimension centers on microscale parameter regulation, reaction medium engineering, and molecular interface reconstruction. Through the synergistic effect of multiple factors, it breaks through the limitations of traditional macroscopic homogeneous synthesis and fundamentally optimizes the nucleation kinetics and growth behavior of materials. It serves as a fundamental and critical physicochemical strategy for the controllable preparation of high-performance nanomaterials.

### 2.1 Local concentration regulation

As one of the core fundamental strategies for regulating local physical and chemical environments, local concentration control is fundamentally different from the extensive concentration adjustment employed in macroscopic systems of traditional synthesis. Traditional approaches only use concentration as a single variable to accelerate or slow down the overall reaction, whereas local concentration control from the perspective of microenvironment engineering involves constructing precise microregional concentration gradients or enrichment environments within a macroscopic system. This

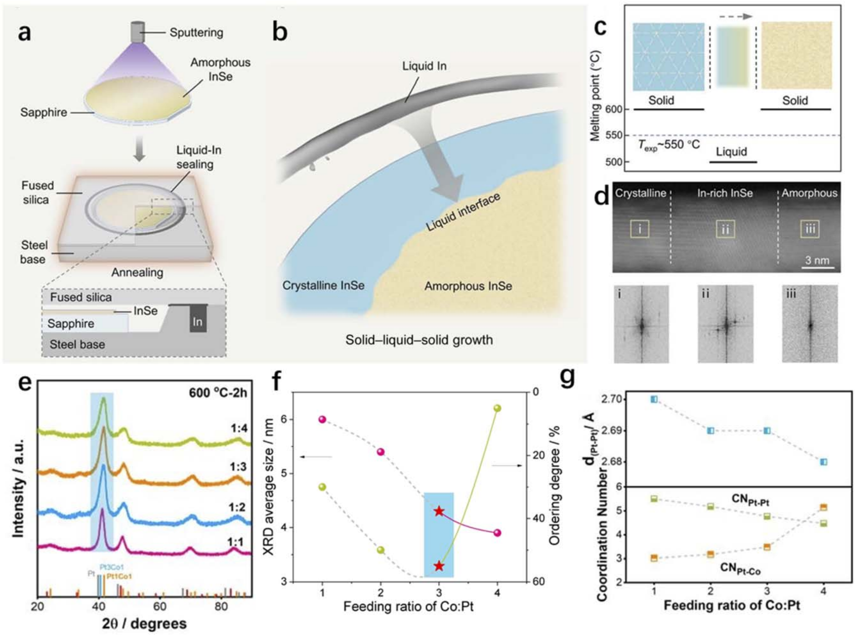

Fig. 2 (a) Amorphous InSe films are deposited on a single-crystal sapphire substrate by means of magnetron sputtering. (b) Zoomed-in diagram of the SLS growth in (a). Liquid In evaporated to create an In-rich interface between amorphous and crystalline InSe. At this interface, the amorphous solid continuously transformed into a crystalline InSe film. (c) Schematic of SLS evolution. At the experimental temperature ($T_{exp}$ ~550 °C), only the In-rich interface is in liquid state, promoting recrystallization by enhancing atomic diffusion and lowering the formation energy. (d) Cross-sectional STEM image and corresponding FFT patterns, showing the presence of the In-rich interface between amorphous and crystalline InSe regions. (e) XRD patterns of Pt-SD/Co–X annealed at 600 °C for 2 h. (f) Corresponding simulated coordination numbers of Pt–Pt. (g) XRD size and ordering degrees for the PtCo-IMC/C-600 samples as a function of feeding ratios of Co : Pt.

provides directional thermodynamic driving forces and kinetic regulation methods for the nucleation and growth of nanomaterials.[70] The core commonality shared by this strategy and other in-dimension approaches such as local temperature control and special solvent regulation lies in reconstructing the chemical conditions of the microreaction field, breaking through the homogeneous limitations of conventional synthesis, and realizing the precise construction of nanomaterials.

This strategy of achieving precise control through local concentration regulation has demonstrated critical value in addressing synthesis bottlenecks for functional materials, particularly in complex systems involving multiphase competition and challenging stoichiometric balance. It provides key insights for overcoming the limitations of traditional preparation methods. This approach has been typically applied in the growth study of high-quality wafer-scale indium selenide (InSe) films. Liu's team developed a solid–liquid–solid (SLS) strategy that synergistically regulates local indium concentration through a sealed system and a liquid indium interface (Fig. 2a).[71] On the one hand, the sealed structure suppresses component loss caused by the high vapor pressure of selenium, strictly maintaining the In : Se = 1 : 1 stoichiometric ratio (Fig. 2b). On the other hand, the liquid indium creates an indium-enriched liquid interface between amorphous InSe and crystalline InSe, reducing the atomic diffusion energy barrier (Fig. 2c). Since amorphous InSe has a higher formation energy, driven by the indium-enriched interface, In and Se atoms rapidly dissolve and precipitate on the crystalline side, ensuring the ABC layered stacking order of InSe (Fig. 2d). The resulting ∼5 cm InSe wafer exhibited a surface roughness reduction from 415 pm (amorphous state) to 37 pm (crystalline state). Laue diffraction and second-harmonic generation confirmed its single-crystal characteristics. Transistor arrays based on this wafer demonstrated an average mobility of 287 $cm^2 V^{-1} s^{-1}$ and a subthreshold swing as low as 67.3 mV $dec^{-1}$, laying the foundation for the large-scale production of two-dimensional channel materials for next-generation integrated circuits.

The core logic of achieving precise material synthesis and phase control through regulating local concentration or concentration gradients is not confined to two-dimensional atomic-scale semiconductor systems. It also demonstrates powerful efficacy in the structural optimization and performance regulation of multi-component alloys. Yang's team proposed a concentration gradient-driven atomic diffusion strategy, constructing a gradient local cobalt concentration environment around Pt seeds (Pt-SD) by adjusting the Co/Pt feeding molar ratio (from 1 : 1 to 4 : 1).[72] This regulation not only overcame the kinetic barriers of atomic diffusion, enabling the synthesis of high-loading, sub-5 nm $L1_0$-type PtCo intermetallic compounds (PtCo-IMC/C) at a relatively low temperature of 600 °C, thereby avoiding particle agglomeration caused by conventional high-temperature annealing (Fig. 2e), but also utilized *in situ* formed Co nanoparticles under local high Co concentration to act as spatial isolators, further suppressing the migration and fusion of PtCo particles (Fig. 2f). X-ray absorption fine structure and molecular dynamics simulations confirmed that the high Co concentration gradient accelerates the penetration of Co atoms into the Pt lattice, resulting in shortened Pt–Pt bond lengths and increased Pt–Co coordination numbers (Fig. 2g). The optimized catalyst exhibited exceptional performance in membrane electrode assemblies, achieving a maximum power density of 1.15 W $cm^{-2}$ at a low Pt loading, with only a 6 mV voltage loss after 30 000 accelerated stress test cycles.

From solid-state synthesis of inorganic materials to solution-phase self-assembly of biomolecules, the general synthetic principle of local concentration regulation has been well demonstrated. Based on this, Yu *et al.* reported a biomimetic strategy for the synthesis of peptide nanocapsules *via* a one-step template-free solvent exchange method: acetone was rapidly injected into an aqueous solution of insect cuticular peptides, and the transient concentration gradient formed during diffusive mixing served as the core driving force for assembly.[73] The process follows a two-stage mechanism: first, the inflow of acetone triggers liquid–liquid phase separation, instantly forming peptide-rich liquid microdroplets; over hundreds of seconds, peptide molecules are thermodynamically driven to localize at the gradient interface and undergo conformational rearrangement to form a β-sheet network, which solidifies the microdroplets into stable hollow nanocapsules. Using this method, three capsule-forming peptides were identified. Microdroplet formation occurred at a water/acetone ratio of 1 : 9 to 1 : 8, and the conversion from microdroplets to capsules was completed within 6 minutes. The encapsulation efficiency for biomacromolecules exceeded 85%, cell viability remained above 90% at a concentration of 400 μg $mL^{-1}$, and mRNA delivery efficiency surpassed 90% after peptide sequence modification. In contrast to the traditional nanoprecipitation method, which requires excessive toxic solvents and only produces solid polymeric nanoparticles, the present method employs mild acetone solvent that preserves biomacromolecule activity. The peptide source is natural and exhibits superior biocompatibility, and the strategy enables co-encapsulation of both hydrophilic and hydrophobic substances.

In summary, as a core strategy for the regulation of local physicochemical environments, the unique characteristic of local concentration control lies in the microscale precise design of concentration, which addresses the key bottlenecks in traditional synthesis such as multiphase competition and stoichiometric imbalance. This strategy is universal across various material systems, including inorganic semiconductors, multi-component alloys, and biomolecular assembly systems.[74] By establishing microregional concentration environments, local concentration control deepens the understanding of material formation mechanisms and realizes a paradigm shift from macroscopic mixing to microscopic manipulation. It provides a design pathway from the concentration dimension for the regulation of local physicochemical environments.[75]

### 2.2 Local temperature regulation

As another core strategy for the regulation of local physical and chemical environments, local temperature control serves as an

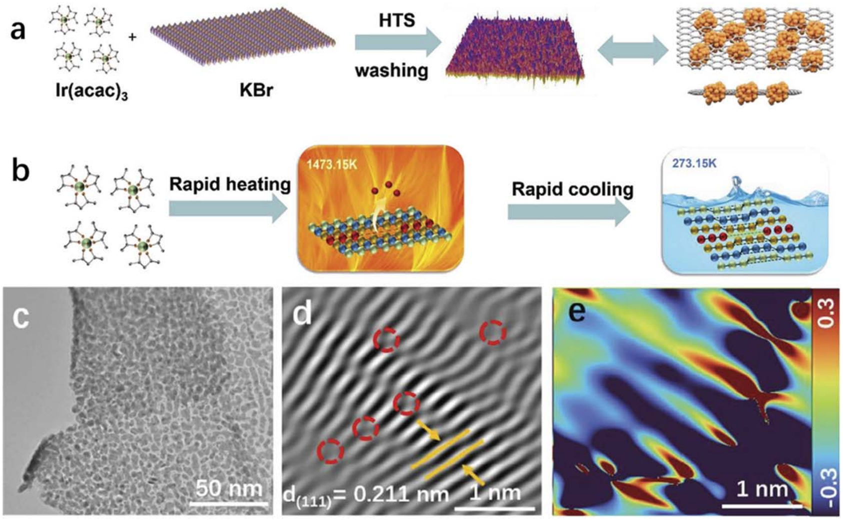

Fig. 3 (a) Synthesis process and coplanar structure diagram of Dr-Ir/C NSs. (b) Frank partial dislocation generation schematic. (c) TEM image of Dr-Ir/C NSs. (d) IFFT patterns of the (111) plane of Dr-Ir/C NSs, exhibiting numerous Frank partial dislocations marked with red circles, respectively. (e) Strain distributions of $e_{xx}$, which is related to the (111) plane.

important complement to local concentration control within the same dimension, both aiming to reconstruct the physical and chemical conditions of the microreaction field.[76] Different from the extensive mode of global homogeneous heating in traditional synthesis, local temperature control from the perspective of microenvironment engineering realizes spatially and temporally precise non-equilibrium temperature variations at the microscale, establishing a thermodynamic non-equilibrium state. This allows the introduction of crystal defects, strain, or metastable phase structures, resolves the inherent contradiction between thermodynamic feasibility and kinetic efficiency in conventional synthesis, and opens a new route for the precise construction of material structures.

Lai's work employed a non-equilibrium high-temperature thermal shock method (>1200 °C) combined with KBr template technology to synthesize coplanar Ir/C ultrathin nanosheets with Frank partial dislocations (Fig. 3a and b).[77] Under instantaneous extreme temperature conditions, Ir precursors were rapidly reduced into Ir nanoparticles, while partial carbon sources were carbonized and grown on the KBr template, forming a coplanar carbon layer that embedded the Ir nanoparticles (Fig. 3c). During this process, the extremely high heating rate induced thermal migration and volatilization of Ir atoms, generating numerous transient vacancies. The subsequent rapid cooling created substantial thermal stress due to the dramatic temperature gradient, causing vacancy collapse and thereby forming abundant Frank partial dislocations within the Ir nanoparticles (Fig. 3d and e). These dislocations introduced approximately 4% compressive strain, which theoretical calculations confirmed could optimize the adsorption free energy of Ir toward hydrogen intermediates by weakening the overly strong H* adsorption, significantly enhancing the intrinsic activity for the hydrogen evolution reaction (HER). Thus, the extreme local temperature variation served as the key driver for generating and freezing these high-density crystal defects, creating a non-equilibrium state that preserved defect structures unstable at room temperature, ultimately achieving breakthroughs in catalyst structure and performance.

In Yuan's study, precise and rapid local temperature regulation played a crucial role in synthesizing metastable multi-element nanoalloys.[78] The core mechanism involved replacing traditional equilibrium processes with non-equilibrium thermodynamic pathways. Specifically, by applying instantaneous high-temperature pulses, the system acquired substantial energy within an extremely short time, promoting rapid decomposition of metal salt precursors into highly active atoms or nanoclusters while creating conditions for their uniform distribution on carbon substrates. The subsequent ultra-fast cooling process (to room temperature within ∼8 s) was key to forming metastable structures—it severely restricted the ability of metal atoms with different radii to undergo long-range diffusion and ordered arrangement, preventing them from reaching thermodynamically stable positions with the lowest energy. This kinetic freezing effect successfully trapped the alloy in a metastable single-phase structure rich in lattice distortions, dislocations, and defects. Meanwhile, the entire synthesis process was completed within an extremely short duration (∼18 s), effectively suppressing sintering and coarsening caused by Ostwald ripening among nanoparticles, thereby yielding ultrafine and uniformly distributed nanoparticles. Consequently, the extreme rapid variation in local temperature not only drove uniform elemental mixing but also served as the decisive factor in constructing metastable microstructures and endowing the materials with excellent electrochemical performance.

In summary, as a core strategy for the regulation of local physicochemical environments, the unique characteristic of local temperature control lies in achieving non-equilibrium regulation through microscale extreme temperature variations, optimizing material properties by introducing structural features such as crystal defects and strain. The local

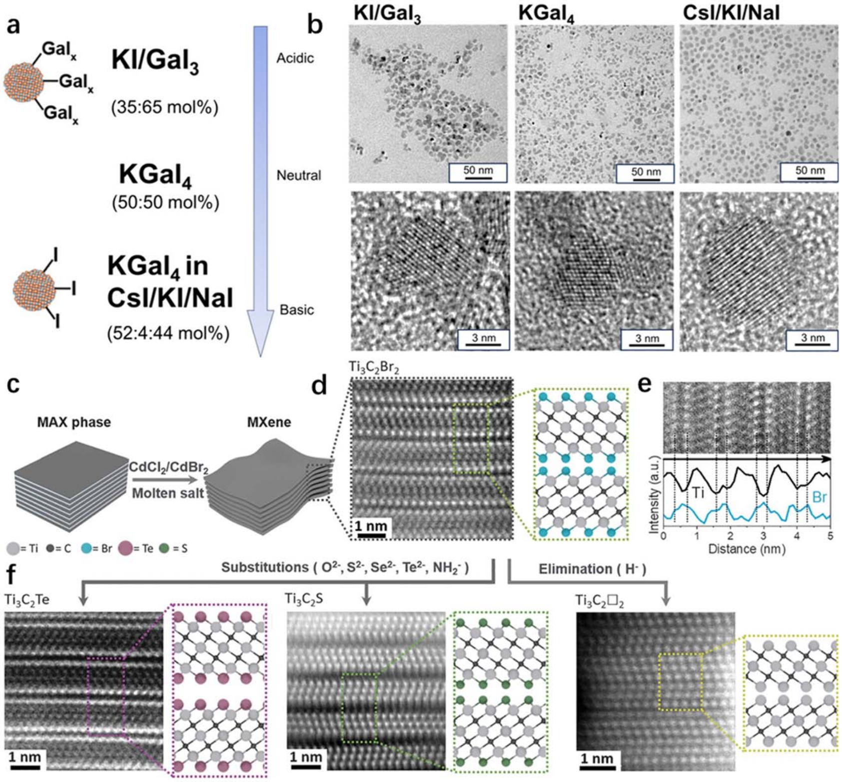

Fig. 4 (a) Scheme showing the nomenclature of Lewis acidic, neutral, and basic molten salts and the effect of acidity on the NC surface terminations. (b) TEM images and HRTEM images of GaAs NCs synthesized in different molten salts. (c) Schematics for etching of MAX phases in Lewis acidic molten salts. (d) HAADF image of $Ti_3C_2Br_2$ MXene sheets synthesized by etching the $Ti_3AlC_2$ MAX phase in $CdBr_2$ molten salt. (e) Energy-dispersive X-ray elemental analysis (line scan) of $Ti_3C_2Br_2$ MXene sheets. HAADF images of (f) $Ti_3C_2Te$ and (g) $Ti_3C_2S$ MXenes obtained by substituting Br for Te and S surface groups, respectively. HAADF image of $Ti_3C_2\square_2$ MXenes (□ stands for the vacancy) obtained by reductive elimination of Br surface groups (right).

temperature control upgrades temperature regulation from the macroscopic global level to precise microscale spatiotemporal manipulation. The concept of realizing precise material construction *via* microscale design of a single physical/chemical parameter further enriches the design dimensions of local physicochemical environment regulation.

### 2.3 Molten salts as solvents

As an innovative strategy based on special reaction media within local physicochemical environment regulation, molten salt solvent regulation falls into the same local physicochemical dimension as the aforementioned local concentration and temperature regulation. Their core commonality is achieving precise nanomaterial synthesis by reconstructing the physical and chemical conditions of the microreaction field. Different from the solubilization function of single solvents in traditional synthesis, molten salt solvents, from the perspective of micro-environment engineering, feature a unique ionic structure, a wide liquid temperature window, and tunable Lewis acidity/basicity, upgrading the role of solvents from merely dissolving precursors to an essential component of the microreaction field. By tuning the nucleation, growth, and surface properties of materials *via* the inherent physicochemical characteristics of the solvent, molten salt regulation opens a new route for the synthesis of high-quality and structurally precise nanomaterials.[79]

In the synthesis of III–V semiconductor quantum dots, Talapin *et al.* developed a dehalosilylation reaction strategy based on molten salts (Fig. 4a).[80] The process begins by mixing group III halides (*e.g.*, $GaI_3$ and $InBr_3$) with $(Me_3Si)_3Pn$ (Pn = P, As) precursors in molten inorganic salts, followed by reaction at high temperatures *via* hot injection or heating to generate III–V nanocrystals. The molten salts serve not only as thermally stable solvents but also effectively prevent side reactions between strongly Lewis acidic gallium precursors and solvents due to their chemical inertness. More importantly, by modulating the Lewis acidity/basicity of the molten salts, such as acidic $KI/GaI_3$, neutral $KGa_4I$, or basic CsI/KI/NaI systems, the surface termination modes, morphological evolution, and size distribution of the nanocrystals can be significantly influenced (Fig. 4b). This dehalosilylation reaction, which involves no oxidation state changes and represents a typical metathesis reaction, is applicable to synthesizing GaAs, GaP, InP, InAs, and their ternary alloy quantum dots. The high-temperature conditions are crucial for annealing structural defects, with Raman spectroscopy and PXRD results consistently demonstrating that nanocrystals synthesized at elevated temperatures exhibit higher crystallinity and fewer point defects. After reaction completion, the nanocrystals can be recovered by dissolving the salt matrix in organic solvents and further modified with long-chain ligands such as oleylamine to form colloidally stable dispersions in nonpolar solvents.

Furthermore, the solvent functionality of molten salts extends beyond providing high-temperature environments, as their powerful ion-exchange capability demonstrates significant potential in precise surface engineering of two-dimensional materials. In another pioneering work, Talapin *et al.* developed a universal molten salt-based strategy for covalent surface functionalization of MXene materials.[81] This pathway consists of two key stages: first, Lewis acidic molten salts (*e.g.*, $CdCl_2$ and $CdBr_2$) are used at high temperatures to etch MAX phase precursors, selectively removing aluminum layers to produce MXene intermediates with pure halogen-terminated surfaces. This step effectively avoids common side reactions such as oxidation and hydrolysis encountered in aqueous etching, ensuring homogeneous surface terminations with high reactivity (Fig. 4c–e). Subsequently, these halogen-terminated MXenes undergo high-temperature ion-exchange reactions with nucleophiles (*e.g.*, $Li_2Te$, $Li_2S$, and $NaNH_2$) in another molten alkali metal halide system (Fig. 4f). Here, the molten salts not only serve as high-temperature ionic solvents and reaction media but also induce MXene interlayer "swelling" to increase interlayer spacing, enabling even bulky ions such as $Te^{2-}$ to access and replace original halogen ions. This allows precise conversion to various terminal structures including O, S, Se, Te, NH, and even bare surfaces. This strategy not only expands the chemical diversity of MXenes but also effectively regulates their lattice strain (*e.g.*, >18% in-plane expansion induced by Te termination) and electronic properties (*e.g.*, superconductivity in $Nb_2CT_n$), demonstrating powerful potential for the rational design of 2D materials.

In summary, molten salts function as a multifunctional reaction platform in nanomaterial synthesis that far surpasses conventional solvents. Their core value lies in three key aspects: first, their high-temperature stability provides an indispensable environment for perfect crystal growth and defect repair; second, their tunable Lewis acidity/basicity offers a crucial means for precise regulation of material surface chemistry; third, their unique ionic environment not only facilitates efficient mass transport but also imparts distinctive colloidal stabilization capabilities to the system. These characteristics collectively enable the efficient execution of various reaction mechanisms—including metathesis and ion exchange—based on molten salts, thereby significantly expanding the synthetic dimensions and application prospects of functional nanomaterials.[82] The aforementioned research strongly demonstrates that the molten salt strategy has emerged as a key enabling technology, driving nanomaterials toward a new era characterized by high crystallinity, controllable microstructure, and customizable functionality.

### 2.4 Liquid metals as solvents

As another core strategy based on special reaction media for local physicochemical environment regulation, it exhibits unique and powerful potential in the field of material synthesis. Compared to conventional solvent systems, liquid metals overcome multiple limitations including restricted solubility, inadequate crystal morphology control, and challenges in product separation.[83] Their distinctive value lies in three aspects: they not only possess exceptional metal dissolution capacity but also actively guide crystal growth directions through interfacial interactions, creating anisotropic thermodynamic environments; meanwhile, their surface properties can be tuned *in situ via* external fields, providing dynamically adjustable interfacial microenvironments for material synthesis and separation.[84] This dual-function platform, serving as both solvent and template, offers novel conceptual and practical pathways for developing advanced material preparation strategies.

In the synthesis of metals and alloy crystals, liquid metals function as efficient "metal solvents". Researchers dissolve target metal solutes (*e.g.*, Zn, Sn, and Ag) in liquid gallium under heating to form homogeneous alloys, subsequently inducing supersaturated precipitation during cooling to achieve crystal nucleation and growth within the liquid metal (Fig. 5a).[85] A key breakthrough of this method lies in resolving the product separation challenge in high-surface-tension solvents: the team innovatively combined electrocapillary modulation with vacuum filtration, applying an electric field to reduce the surface tension of liquid gallium to near zero, enabling its penetration through filter membranes and successful collection of intact, structurally precise crystals. Crucially, the liquid metal solvent is not an inert medium; it exerts critical structure-directing effects on crystal growth through facet-specific interfacial energy differences with different crystal planes. Theoretical simulations confirm that, for instance, Zn's (0001) plane remains more stable due to weaker interactions with liquid gallium, directly promoting preferential growth of hexagonal zinc platelets with remarkable symmetry. By systematically adjusting solute concentration, temperature, pressure, or introducing tertiary components (*e.g.*, In), growth kinetics can be precisely regulated to achieve controlled synthesis of diverse morphologies ranging from simple fractals and complex dendrites to regular cubes. This platform can produce not only elemental metal crystals but also intermetallic compounds such as $Ag_2Ga$ and $Al_{11}Mn_4$, which exhibit significant application potential in gas sensing, piezoelectric responses, and photocatalysis.

Another study innovatively utilized room-temperature liquid metals as a reactive environment to successfully synthesize two-dimensional metal oxides that are challenging to produce through conventional methods, such as $HfO_2$, $Al_2O_3$, and $Gd_2O_3$.[86] The synthesis mechanism is rooted in thermodynamic driving forces: when target metal elements (*e.g.*, Hf, Al, and Gd) are co-alloyed into the liquid metal, they selectively and preferentially oxidize at the alloy surface due to the more negative Gibbs free energy of their corresponding oxides, forming a self-limiting ultrathin oxide layer. To isolate the oxide layer, researchers developed two methods: first, the van der Waals exfoliation method (Fig. 5b), which transfers the oxide layer from the liquid metal surface *via* substrate contact, yielding

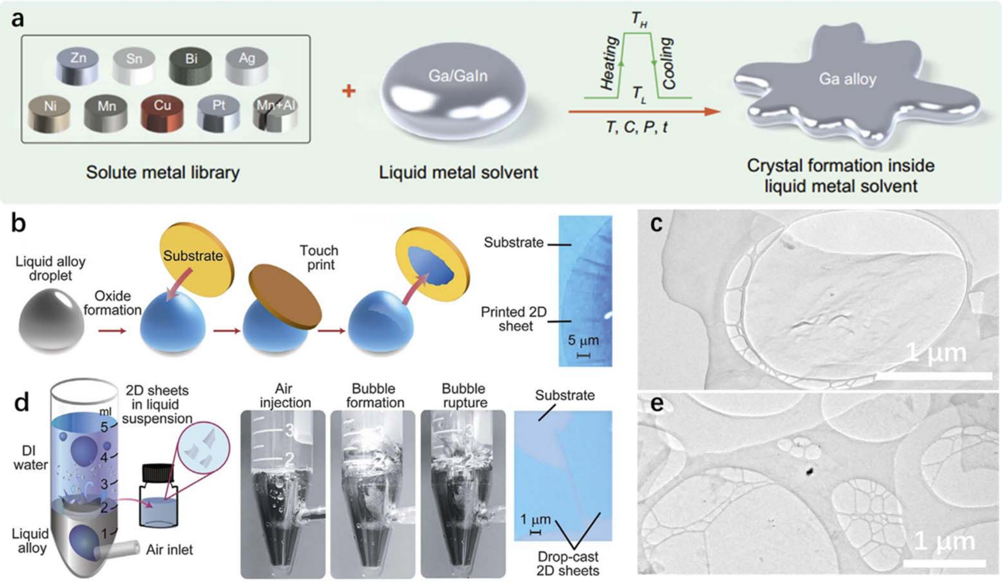

Fig. 5 (a) Experimental procedures to grow metal crystals in a liquid metal solvent. Solute metal, solvent metal, and the parameters (including temperature $T$, concentration $C$, pressure $P$, and time $t$) that determine the crystal structure and size are indicated. (b) Schematic representation of the van der Waals exfoliation technique. The pristine liquid metal droplet is first exposed to an oxygen-containing environment. Touching the liquid metal with a suitable substrate allows transfer of the interfacial oxide layer. An optical image is shown at the right. (c) Characterization of materials derived from the exfoliation method. Alloys containing approximately 1% of added hafnium. (d) Schematic representation of the gas injection method (left), photographs of the bubble bursting through the liquid metal (center), and an optical image of the resulting sheets drop-cast onto a $SiO_2$/Si wafer (right). (e) Characterization of materials derived from the gas injection method. Alloy containing approximately 1% of added hafnium.

highly crystalline, substrate-supported 2D oxides free of inclusions suitable for electronic devices (Fig. 5c); second, the gas injection method (Fig. 5d), which introduces pressurized air into the liquid metal, utilizing bubbles to carry and disperse the oxide layers into water as suspensions, enabling high-yield synthesis—ideal for energy storage devices (Fig. 5e). These strategies ingeniously leverage the fluid, isotropic surface of liquid metals and the weak van der Waals interactions between the metals and their solid oxides, creating ideal conditions for obtaining intact, clean 2D crystals. This approach enables the universal synthesis of non-layered oxides, providing a new materials platform for high-performance electronic devices.

In summary, as an important branch of medium-based strategies for local physicochemical environment regulation, liquid metal solvent regulation is uniquely characterized by the bifunctional microenvironment design of "solvent + template". It also enables dynamic regulation of interfacial properties *via* external fields, overcoming the limitations of both conventional solvents and single templating methods. The liquid metal solvent strategy further enriches the design dimension of reaction media in local physicochemical environment regulation. The evolution of local physicochemical environment regulation, from physicochemical parameter tuning to reaction medium engineering, provides robust methodological support for the precise structural tailoring and function-oriented preparation of materials. It is expected to drive innovative advances in future materials design and manufacturing technologies.[87]

### 2.5 Ligand regulation

As a molecular-scale refined strategy for local physicochemical environment regulation, the role of ligands has long gone beyond their conventional function as stabilizers against agglomeration. In fact, ligands have evolved into chemical directors that can program material structures at the molecular level.[88] By precisely regulating the transformation pathways of reaction precursors, the coordination states of intermediates, and their adsorption behaviors on specific crystal facets, the microchemical environment constructed by ligands fundamentally governs the nucleation, growth kinetics, and final structural features of nanocrystals. This enables precise control over the size, morphology, crystal phase, and composition of the materials.

The first dimension of ligand functionality manifests in the precise navigation of material growth pathways. In Owen's study, a tunable synthesis method based on substituted thiourea precursors was reported for preparing metal sulfide nanocrystals (Fig. 6a and b).[89] The synthesis involves reacting substituted thioureas with metal salts in an organic solvent, generating metal sulfide monomers through precursor conversion, followed by homogeneous nucleation and growth. The conversion kinetics of thiourea are critical: its conversion rate is modulated by the electronic and steric effects of substituents, thereby controlling the monomer supply rate. Faster conversion leads to higher nucleation density and smaller nanocrystal sizes, ultimately achieving size control upon complete conversion. Ligands play a vital role in the synthesis by fine-tuning the

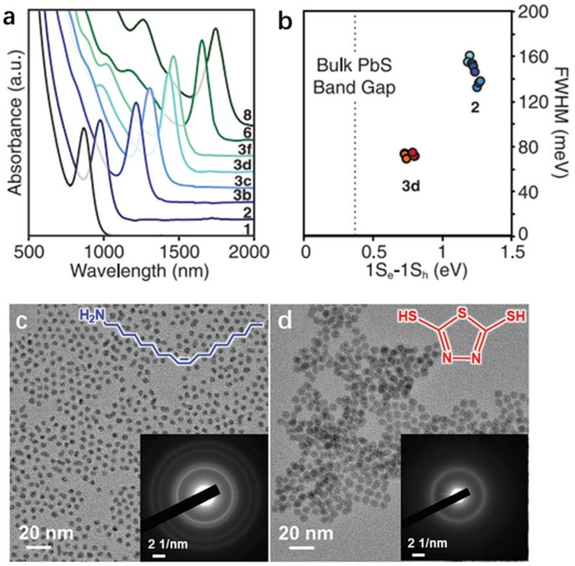

Fig. 6 (a) Ultraviolet-visible-near-infrared absorption spectra of PbS nanocrystals synthesized using substituted thioureas. (b) Results of a reproducibility study showing the nanocrystal diameter and relative size distribution of three reactions for two different precursors. (c) TEM image of Pd NPs-OAm. Insets: molecular structure of oleylamine (top) and the corresponding SAED pattern of Pd NPs-OAm (bottom). (d) TEM image of Pd NPs-Bis-24h. Insets: molecular structure of bismuthiol I (top) and the corresponding SAED pattern of Pd NPs-Bis-24h (bottom).

microenvironment: they not only act as surfactants stabilizing the nanocrystals but also regulate precursor reaction kinetics by influencing the local chemical environment, thereby precisely controlling nucleation and growth processes to ensure monodispersity and high batch-to-batch consistency. The significance of this work lies in demonstrating that precise regulation of reaction microenvironment dynamics through ligand chemistry enables tailored design of nanocrystal size and high-yield synthesis.

If the aforementioned studies demonstrate ligands' role as regulators of reaction kinetics, guiding material growth by controlling precursor conversion rates, the following work reveals an even more profound capability: the direct intervention and permanent alteration of the crystal structure in already-nucleated nanomaterials. Zhang's team reported a strategy for achieving amorphousization of palladium nanomaterials under ambient conditions through ingenious ligand engineering.[90] The synthesis begins with well-defined crystalline palladium nanomaterials, followed by postsynthetic ligand exchange where original surface ligands are replaced by distinctive bismuth-thiol I compounds (Fig. 6c and d). The mechanism fundamentally relies on the ligand-induced reconstruction of the interfacial microenvironment: the strong coordination between sulfur atoms in bismuth-thiol I and palladium surfaces generates intense interactions sufficient to disrupt the lattice order of surface palladium atoms, inducing a crystal-to-amorphous transition. Here, ligands transcend mere surface stabilization to function as critical “microenvironment reconstructors”, creating a sulfur-rich chemical environment at the interface that drastically perturbs and ultimately collapses the metal lattice, endowing the material with exceptional electrocatalytic hydrogen evolution performance. This work's significance lies in revealing ligands as powerful agents for microenvironment reconstruction that directly intervene in and alter materials' bulk phase structure and properties, opening new pathways for synthesizing novel metastable phase nanomaterials.

In summary, the above studies systematically demonstrate the multilevel regulatory ability of ligands in material synthesis from two perspectives: reaction kinetics guidance and interfacial microenvironment reconstruction. Together, they delineate a complete ligand engineering spectrum spanning growth process direction to bulk structure intervention, profoundly revealing that material properties are determined not only by chemical composition but more critically by the microscopic structure and electronic states governed by ligands.[91] Looking forward, the deep integration of artificial intelligence with advanced *in situ* characterization technologies will progressively transform our understanding of coordination microenvironments from empirical knowledge to rational design. Ligand engineering is poised to evolve into a programmable language for materials orientation, where precise molecular-level coordination instructions can be encoded to design next-generation functional materials with tailored properties, ultimately advancing nanosynthesis from empirical exploration to scientific construction.

## 3 Spatial confinement effects

The spatial confinement effect is an important dimension for microenvironment regulation in nanomaterial synthesis. By constructing exclusive microscale physical confined spaces, it provides directional spatial guidance for nucleation and assembly of materials, enabling precise control over material morphology, structure and dimensionality. This dimension takes static rigid confinement, dynamic flexible regulation, and their synergistic integration as the core design logic. Through physical constraint and mass transport optimization in confined spaces, it guides materials to form regular and complex hierarchical structures, serving as a core spatial regulation strategy for the synthesis of nanomaterials with diverse structures and specific functions.

### 3.1 Hard templating method

As a fundamental and core strategy for regulating spatial confinement effects, the hard-template method is a typical implementation of physical spatial confinement in microenvironment engineering, which is fundamentally different from the random nucleation and growth mode in traditional synthesis. Traditional synthesis lacks spatial constraints on nucleation and growth, easily leading to structural inhomogeneity.[92] In contrast, from the perspective of microenvironment engineering, the hard-template method achieves top-down physical spatial confinement of the microreaction field

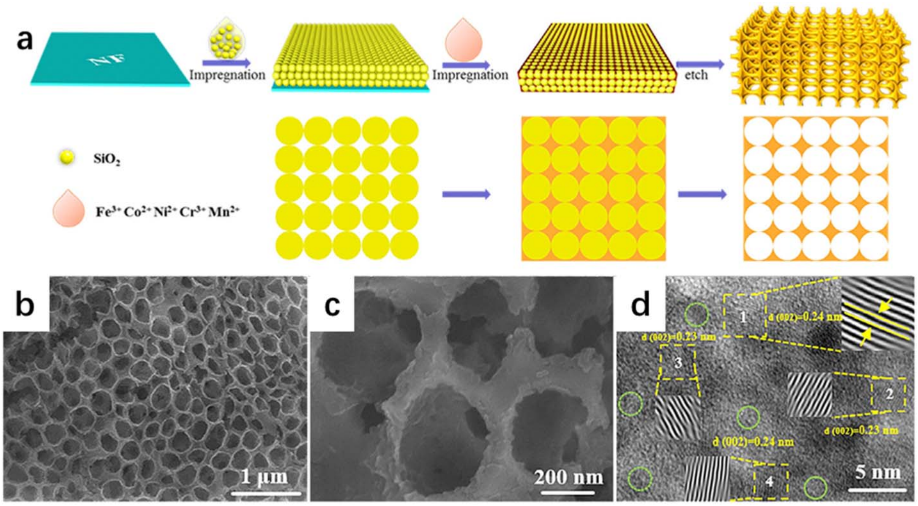

Fig. 7 (a) Schematic diagram of the synthesis of 3D ordered macroporous HEH. (b) SEM image, (c) TEM image, and (d) HRTEM image.

through the precise design of rigid templates. Meanwhile, it regulates the interfacial microenvironment by combining the chemical properties of the template. By constructing a microreaction field *via* spatial confinement, it directionally controls the nucleation, growth, and assembly of materials.

This advantage is fully demonstrated in electrocatalytic material design. Wang and colleagues synthesized a 3D ordered macroporous high-entropy hydroxide (3DOM-HEH) using the hard templating method. The specific process involved sequentially loading $SiO_2$ nanospheres as hard templates with metal salt solutions onto nickel foam, followed by *in situ* chemical etching and growth in a NaOH solution, where the pore structure was precisely controlled by adjusting the amount of $SiO_2$ used (Fig. 7a).[92] The synthesis mechanism relies on the spatial confinement effect of the hard template. The etching process forms an ordered macroporous structure that not only maximizes the exposure of active sites and facilitates bubble transport but also modulates the microenvironment by altering the spatial curvature of the catalyst (Fig. 7b–d). For instance, finite element analysis indicated that the 3DOM structure enhances the local electrostatic field, increasing the $OH^-$ adsorption concentration by five orders of magnitude, thereby optimizing reaction kinetics. Simultaneously, the strong orbital coupling induced by the high-entropy effect modulates the electronic structure, enabling selective adsorption of $OH^-$ at Fe sites while suppressing $Cl^-$ adsorption, further enhancing catalytic activity and stability. The critical role of the hard templating method in this process lies in constructing ordered channels that directly regulate the electric field distribution, ion enrichment, and mass transfer efficiency within the microenvironment, ultimately achieving efficient water/seawater oxidation performance.

From the construction of three-dimensional ordered macrostructures to the optimization of mass transport pathways at the mesoscale, the application of hard templating demonstrates powerful multi-scale regulation capabilities. In Lotsch's work, researchers successfully synthesized hierarchically porous Covalent Organic Frameworks (COFs) *via* the hard templating method.[93] First, under solvothermal conditions, pre-synthesized ZnO nanoparticles were mixed with COF precursors as hard templates, allowing the COF to grow around the templates to form ZnO@COF composites. Subsequently, the ZnO templates were gently removed by acetic acid etching, creating secondary mesopores approximately 17–20 nm in size while preserving the intrinsic structural mesoporosity of the COF. The synthesis mechanism relies on the solubility of ZnO under acidic conditions, enabling complete template removal without compromising the crystallinity or chemical structure of the COF (Fig. 8a). The critical role of hard templating here lies in precisely constructing mesoscale secondary channels, which significantly optimize mass transport behavior within the material from a microenvironment perspective: The formed hierarchical pores not only

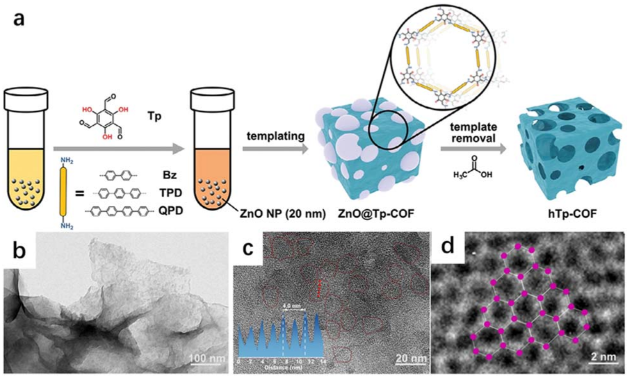

Fig. 8 (a) Synthesis scheme of a template-induced approach toward hierarchical porosity in β-ketoenamine COFs. (b) Low-magnification TEM image of $Ni_3(HITP)_2$/NUS-8 nanosheets. (c and d) HAADF-STEM image of the $Ni_3(HITP)_2$/NUS-8 nanosheet. The inset in (c) shows the intensity line profile of the lattice indicated by the red dashed lines. The inset in (d) depicts the schematic illustration of the $Ni_3(HITP)_2$/NUS-8 framework viewed from the *c* direction.

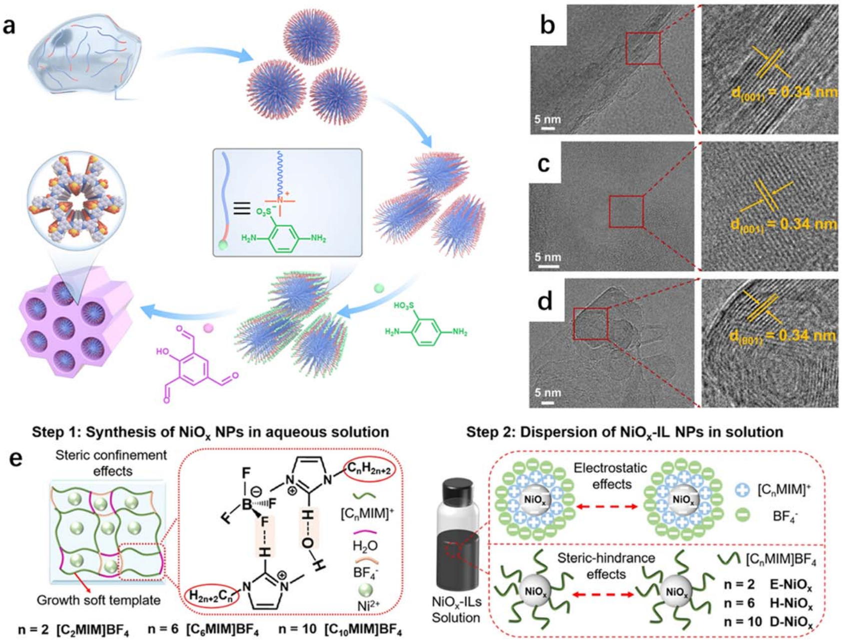

Fig. 9 (a) Synthesis of OHMMCOF-DTAB/OHMMCOF-OTAB. Illustration of the synthesis of off-template pre-products of ordered hierarchical microporous/mesoporous OHMMCOF-DTAB/OHMMCOF-OTAB. HRTEM images: (b) MPCOF, (c) OHMMCOF-DTAB, and (d) OHMMCOF-OTAB. (e) Schematic of the process of ILs as soft templates to assist the synthesis of $NiO_x$ NPs and the $[C_6MIM]BF_4$-assisted dispersion of $NiO_x$ NPs in aqueous solution.

substantially increase pore volume and adsorption capacity but also, by constructing continuous multiscale pore networks, enhance the diffusion coefficient of guest molecules by three orders of magnitude, approaching the diffusion level in bulk liquid. This greatly alleviates diffusion limitations and improves mass transfer efficiency and activity in catalytic reactions.

Furthermore, the design concept of hard templating extends from the construction of porous frameworks to the regulation of crystal growth and interface engineering on two-dimensional planes. In Yuan's work, a hard templating approach was used to construct a solution-processable Metal–Organic Framework (MOF) on metal–organic framework system ($Ni_3(HITP)_2$/NUS-8) with excellent processability:[94] first, two-dimensional NUS-8 nanosheets served as hard templates, guiding the heterogeneous epitaxial growth of $Ni_3(HITP)_2$/NUS-8 *via* solvothermal methods to form a uniform core–shell structure (Fig. 8b). The synthesis mechanism relies on the lattice matching and surface guidance of NUS-8, promoting the ordered nucleation and growth of $Ni_3(HITP)_2$ along its surface in a Stranski–Krastanov mode (layer–island mixed growth), thereby effectively suppressing the agglomeration of $Ni_3(HITP)_2$ and significantly enhancing the material's dispersibility and film-forming properties (Fig. 8c and d). The key role of hard templating in this process lies in creating a two-dimensional confined microenvironment, which not only regulates the size and distribution of $Ni_3(HITP)_2$ but also enhances electronic coupling and charge transfer through the formation of intimate heterointerfaces. This optimizes the material's conductivity and accessibility to gas adsorption/reaction sites, ultimately achieving highly sensitive and selective room-temperature detection of ultratrace $H_2S$.

In summary, as a systematic methodology for material design, the hard templating method's core value lies in creating unique spatially confined microenvironments through pre-designed nanostructured templates.[95] This confined environment not only precisely regulates the nucleation, growth, and assembly processes of functional materials at the physical scale but, more importantly, alters the chemical microenvironment during material synthesis, including key parameters such as reactant mass transport, interfacial interactions, and electron transfer behavior.[96] Through this synergy of physical spatial confinement and chemical microenvironment regulation, the hard templating method achieves precise construction of material structures across hierarchies from the nanoscale to the macroscale, providing a solid theoretical foundation and methodological support for the design and preparation of new-generation functional materials.

### 3.2 Soft templating method

As a flexible and dynamic strategy for spatial confinement regulation, the soft-template method serves as an important complement and differentiated development to the hard-template method. Both belong to the category of spatial confinement effects, sharing the core principle of constructing microreaction fields *via* spatial confinement to directionally regulate the nucleation and growth of materials. In contrast to the rigid and static spatial constraints of the hard-template method, the soft-template method from the perspective of microenvironment engineering employs self-assembled supramolecular aggregates (such as amphiphilic molecules) as flexible templates. Through weak interfacial interactions including electrostatic forces and hydrogen bonds, it achieves dynamic spatial confinement under mild conditions.[97]

Taking covalent organic frameworks as an example, Ma and colleagues used water as the solvent and introduced two amphiphilic surfactants with different alkyl chain lengths—dodecyltrimethylammonium bromide (DTAB) and octadecyltrimethylammonium bromide (OTAB)—as soft templates to synthesize COFs with ordered hierarchical microporous/mesoporous structures (Fig. 9a).[98] To prevent the templates from being expelled from the COF growth region due to strong crystallization driving forces, an anionic COF skeleton and ionic templates were employed, where the soft templates and the COF are interconnected *via* ionic bonds. Using water as the solvent prevented random distribution of the amphiphilic surfactants while ensuring their hydrophobic self-assembly. The formation of ionic bonds facilitated the introduction and removal of the templates. After detailed screening of ion exchange methods for template removal, hydrogen ions were successfully used to remove the templates while preserving the crystallinity of the ordered hierarchical porous COFs. To obtain COFs with ordered hierarchical microporous/mesoporous structures, smaller building blocks capable of constructing approximately 1.8 nm micropores were selected. After optimizing solvent and catalyst conditions, the pre-product of ordered hierarchical microporous/mesoporous COFs was successfully constructed in an aqueous solution at 120 °C. The building blocks and templates used were 2-hydroxy-1,3,5-benzenetricarboxaldehyde, 2,5-diaminobenzenesulfonic acid, and DTAB/OTAB, with the resulting COFs named OHMMCOF-DTAB and OHMMCOF-OTAB. The key synthesis steps involved dispersing DTAB/OTAB in an aqueous solution to allow self-assembly into spherical micelles with brominated amine hydrophilic terminals (Fig. 9b–d).

Another typical application is evident in the energy materials field. Chen *et al.* introduced multifunctional ionic liquids (ILs), imidazolium tetrafluoroborates ([$C_n$MIM]$BF_4$, specifically 1-ethyl-, 1-hexyl-, and 1-decyl-3-methylimidazolium tetrafluoroborate), as multi-level growth templates to simultaneously regulate the quality of multilayer structures from $NiO_x$ to perovskite films (Fig. 9e).[99] [$C_n$MIM]$BF_4$ acts as a soft growth template by forming an extended hydrogen bonding system. The particle size and crystalline properties of $NiO_x$ nanoparticles are closely related to the alkyl chain length of [$C_n$MIM]. Meanwhile, the electrostatic and stereodirecting effects of [$C_n$MIM]$BF_4$ hinder the aggregation of $NiO_x$ nanoparticles, enabling the preparation of $NiO_x$-IL thin films with excellent solution dispersibility and film-forming uniformity. The crystalline quality of perovskite films deposited on $NiO_x$-IL hole transport layers (HTLs) is significantly improved, along with superior upper interface contact, as the [$C_n$MIM]$BF_4$ attached to the HTLs can further act as a growth template for perovskites by providing nucleation sites.

Overall, the essence of the soft templating method lies in utilizing dynamic supramolecular assemblies as mesoscopic reaction fields to actively guide and dynamically regulate material growth through non-covalent interactions. This approach not only enables precise control over the size, morphology, and pore structure of the products but also, due to its reversible and responsive nature, provides a powerful tool for constructing functional materials with complex hierarchical structures.[100] From molecular self-assembly to mesostructure construction, the soft templating method demonstrates the unique charm of bottom-up synthesis pathways, while also opening new possibilities for future green synthesis and biomimetic material design.

### 3.3 Synergistic soft–hard templating

As an advanced integrated strategy for spatial confinement regulation, the soft–hard template synergistic strategy is an integrated innovation of the two basic strategies (hard template and soft template) within the same dimension. All three strategies share the core goal of constructing microreaction fields *via* spatial confinement.[101] Different from the single spatial regulation mode of single-template strategies, the soft–hard template synergistic strategy under the framework of microenvironment engineering achieves functional complementarity and process synergy through the rigid static confinement of hard templates and the flexible dynamic regulation of soft templates. This solves the problem that single-template methods can hardly achieve stable macroscopic structures and precise microscopic regulation at the same time.

Based on this synergistic concept, researchers have developed various innovative synthesis strategies. Zhang's study employed an innovative "soft–hard coupled assembly" strategy to successfully synthesize porous carbon materials with an internal wrinkling topology (Fig. 10a).[102] The process first uses wrinkled mesoporous silica ($mSiO_2$) as a hard template to define the material's macroscopic spherical morphology and primary macroporous structure; simultaneously, F127 micelles are used as a soft template to introduce small-sized mesopores. The key to the synthesis mechanism lies in the coupling of the two *via* hydrogen bonding to form a composite template, which jointly guides the polymerization and cross-linking of aniline and phytic acid at their interface, forming a three-dimensional polymer precursor. Subsequently, through a precisely controlled carbonization process, the soft template thermally decomposes to generate small mesopores, and the polymer converts into an N-, O-, and P-doped carbon skeleton; finally, alkaline etching removes the hard template, not only replicating its large/macropores but also inverting its inherent "external wrinkling" morphology, successfully constructing a unique "internal wrinkling" structure within the carbon skeleton. This synergistic strategy perfectly integrates the structural rigidity of the hard template with the pore-modulating capability of the soft template, thereby achieving in one step the synergistic construction of hierarchical pores, heteroatom doping, and internal wrinkling morphology, ultimately endowing the material with an extremely high specific surface area and excellent lithium-ion storage performance.

Besides synergistic strategies based on static interfacial interactions, the integration of soft and hard templates *via*

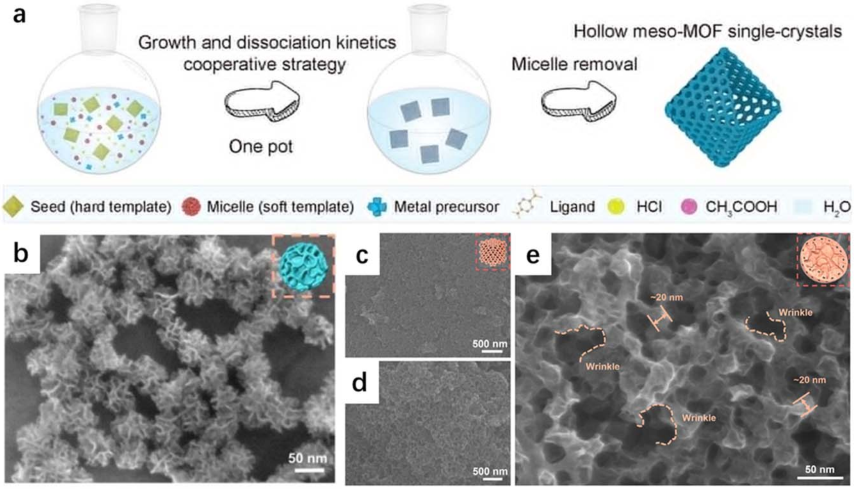

Fig. 10 (a) Schematic of the growth and dissociation kinetics cooperative strategy for the hollow-structured single-crystalline meso-MOFs. (b) FESEM image of highly wrinkled $mSiO_2$ templates. (c–e) FESEM images of the IWPC-H material.

dynamic process regulation also exhibits unique advantages. Zhao and co-workers developed a synergistic strategy of growth and dissociation kinetics, enabling the synthesis of hollow single-crystalline mesoporous MOFs by combining soft and hard templates.[103] Acid-labile Ce-MOFs served as the hard template to provide the morphology and lattice foundation, while Pluronic F127 micelles acted as the soft template to direct mesopore formation (Fig. 10b). This study clearly presented the key parameters and addition sequence of the $HCl/CH_3COOH$ dual-acid regulation system. The optimal ratio for preparation was 4 : 6 (pH ≈ −0.03), and that for hollow open-capsule MOFs was 9 : 1 (pH ≈ −0.29). For acid addition, an aqueous solution of $ZrCl_4$–F127 was first prepared and Ce-UiO-66 seeds were dispersed. The dual acid mixture at the preset ratio was then injected in one shot. After standing for 0.5 h, the ligand was added and the reaction proceeded at 80 °C. Meanwhile, the group performed systematic experiments with gradient acid ratios including 0 : 10, 2 : 8, and 10 : 0, establishing a complete regulatory relationship among acid ratio, pH, kinetic rate, and product structure. Here, HCl lowered the pH and dominated seed dissociation to generate hollow interiors, while $CH_3COOH$ acted as a coordination modulator to tune the crystallization rate of Zr-MOFs and guide the formation of ordered mesopores (Fig. 10c–e). By precisely balancing the seed dissociation kinetics ($k_d$) and shell growth kinetics ($k_g$), synchronous seed dissolution and epitaxial growth of single crystalline mesoporous shells were achieved. This one-step route enabled the construction of hollow single crystalline mesoporous materials with finely tunable structural parameters, overcoming the long-standing challenge in conventional methods of reconciling long-range crystalline order and complex hierarchical structures.

In summary, as an advanced and integrated strategy for spatial confinement regulation, the soft–hard template synergistic strategy is uniquely characterized by realizing cross-scale spatial confinement synergy of rigidity and flexibility, static and dynamic regulation, as well as macroscopic and microscopic scales.[104] This strategy effectively overcomes two major limitations of traditional synthesis methods: firstly, the inherent constraints of single template systems regarding structural complexity and functional integration; secondly, the traditional conflict between macroscopic morphology control and microscopic structure optimization. Through rational synergistic design, researchers can introduce rich hierarchical pores and functional sites while maintaining the material's long-range order, achieving a unification of structural regularity and functional diversity. This integrated structure–function construction strategy provides a universal technical platform for developing a new generation of high-performance nanomaterials, significantly expanding their application prospects in fields such as energy, environment, and catalysis, and demonstrating substantial scientific value and broad application potential.

## 4 External energy environments

The external energy environment is a key dimension for microenvironment regulation in nanomaterial synthesis. Through non-contact, precise microscale energy input, it modifies the energy state, reaction thermodynamics and kinetics in the microreaction zone, enabling flexible control over the material synthesis process. Taking thermal energy input, non-thermal physical field interaction and multi-effect synergistic regulation as core forms, it can efficiently tune the reaction process, crystal structure and interfacial interactions, and expand the synthesis scope and performance boundaries of nanomaterials. It serves as a core energy regulation strategy for the synthesis of high-value-added and novel nanomaterials.

### 4.1 Microwave field-assisted synthesis technology

As one of the core strategies for external energy environment regulation, microwave-assisted synthesis is a typical implementation of precise microscale energy input in microenvironment engineering. It differs fundamentally from the global heating mode in traditional synthesis, which features high energy consumption and slow heating rates: energy input in traditional synthesis lacks selectivity and precision, whereas microwave-assisted synthesis from the perspective of microenvironment engineering achieves rapid conversion from electromagnetic energy to thermal energy *via* its unique bulk heating mechanism. By selectively heating to form microregional "hot spots", it provides precise energy input for the microreaction field. Through the introduction of a non-contact external energy field, it modifies the energy state of the microreaction field and directionally regulates the material synthesis process.[105,106]

Ultrafast microwave synthesis demonstrates significant potential in regulating the interaction between metal nanostructures and supports. In one notable example, Wang *et al.* utilized ultrafast microwave-assisted synthesis to prepare PtRu alloy nanoclusters supported on a two-dimensional $WO_3$-$O_V$ carrier (PtRu/$WO_3$-$O_V$) (Fig. 11a). Owing to the strong synergy between alloying and metal–support interaction, the prepared catalyst exhibited exceptionally high HER activity across a wide pH range.[107] The synthesis began by thoroughly mixing $NaH_2PO_2 \cdot H_2O$, $Pt(acac)_2$, $Ru(acac)_3$, and $WO_3$ hydrate. The mixture was then transferred to a quartz boat, mixed with 30 μL of deionized water, and stirred to form a homogeneous paste. A 60-second microwave-assisted reaction yielded a deep blue powder, which was finally washed at 80 °C to obtain the final sample (Fig. 11b). Microwave radiation alters the wavelength between the air and the mixture, where confined short waves generate a dynamic electric field within the mixture. This field induces violent oscillation of water molecules, thereby efficiently transferring energy to the powder system (Fig. 11c). The internal ionic charge imbalance within $H_2PO_2^-$ and its electromagnetic interaction with the surrounding air generated visible sparks under the microwave field. These localized, extreme-temperature "sparks" instantaneously achieved the mutual dissolution and alloying of Pt and Ru atoms, while simultaneously inducing the formation of more oxygen vacancies ($O_V$) in the $WO_3$ support. This process established a strong metal–support interaction between the PtRu alloy nanoclusters and the $O_V$-rich $WO_3$ carrier.

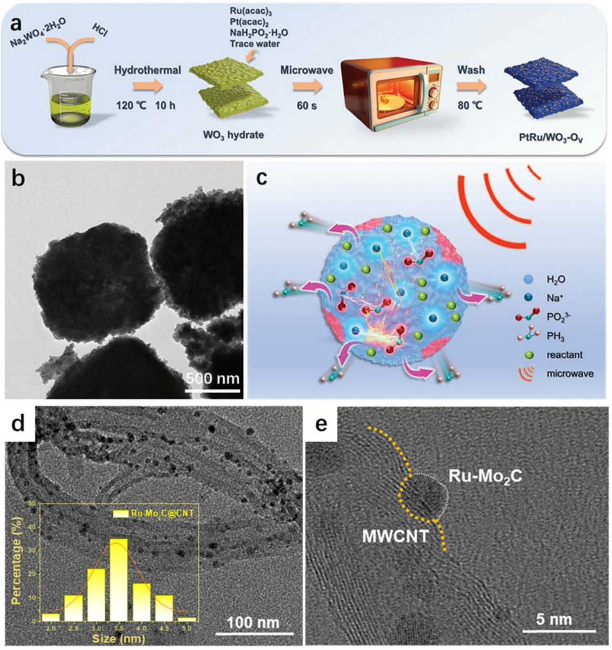

Fig. 11 (a) Synthesis schematic of PtRu/$WO_3$-$O_V$. (b) Low-magnification TEM image of PtRu/$WO_3$-$O_V$. (c) Mechanism of the microwave reaction. (d) TEM image of Ru–$Mo_2C$@CNT, the inset shows the size distribution of nanoparticles. (e) HRTEM image of Ru–$Mo_2C$@CNT.

In the work of Lai *et al.*, a simple, rapid, solvent-free microwave pyrolysis method was employed to one-step synthesize Ru–$M_xC$@CNT (M = Mo, Co, Cr).[108] Acid-treated carbon nanotubes (carboxylated CNTs) were mixed with metal carbonyl salts ($Ru_3(CO)_{12}$ and $M(CO)_x$). Under rapid microwave irradiation, polar functional groups absorbed microwave energy, forming local hot spots. The metal precursors decomposed, producing CO gas, which induced confined carbothermal reduction to metal particles. These particles were anchored at the hot spots, forming a encapsulated structure and establishing a strong metal–support interaction, resulting in a strongly coupled, small-sized supported catalyst (Fig. 11d and e).

The precise structural design and efficient synthesis of such materials ultimately point toward the industrial goal of large-scale production. Liu *et al.* pioneered a microwave pyrolysis strategy using ZIF-67 as a precursor, enabling the rapid and efficient kilogram-scale production of electrocatalysts in a customized reactor.[109] The unique instantaneous volumetric heating and dielectric confinement effects of microwave irradiation not only drastically shorten the pyrolysis time, only 10 min of holding compared with more than 2 hours for heating and holding in traditional calcination, but also achieve an 85% reduction in energy consumption. The mechanism of selective volumetric heating is far superior to conventional thermal conduction/radiation heating in terms of energy efficiency. More importantly, microwave irradiation precisely regulates the structural evolution of the catalyst at the microenvironment level: it effectively suppresses the migration and agglomeration of cobalt species, promoting the coexistence of high-density cobalt single-atom sites (Co–$N_4$) and cobalt nanoparticles (Co NPs). Meanwhile, the localized transient thermal energy induced by microwaves generates unique nanocarbon bridges, which act as "electronic highways" to interconnect the isolated dual active sites. This structural synergy, combined with the optimization of the electronic structure of cobalt sites *via* strong metal–support interactions, significantly reduces the energy barrier of oxygen-involving reactions, endowing the catalyst with outstanding bifunctional oxygen evolution reaction/oxygen reduction reaction activity and stability. The assembled zinc-air batteries exhibit performance far exceeding that of commercial benchmark catalysts. This work provides a new paradigm with atomic precision and industrial feasibility for the efficient and large-scale production of high-performance electrocatalysts and further validates the remarkable advantages of microwave methods over traditional calcination using clear energy consumption and time data.

In summary, microwave-assisted synthesis has transcended its role as merely a rapid synthesis tool; it is fundamentally a scientific means of manipulating reaction microenvironments and material formation pathways through precise energy delivery.[110] Its core value lies in utilizing selective volumetric heating and ultrafast kinetics to actively create reaction conditions conducive to forming nanostructures with small size, high dispersion, and strong interfacial interactions. Looking ahead, with a deeper understanding of the interaction mechanisms between microwaves and matter, coupled with the integrated development of reactor design and intelligent control technologies, microwave synthesis technology is expected to break through the bottlenecks of traditional synthesis and become a disruptive technology leading the green and intelligent manufacturing of next-generation advanced nanomaterials.

### 4.2 Laser-assisted synthesis technology

As a transient extreme energy regulation strategy for external energy environment control, laser-assisted synthesis serves as an important complement to the aforementioned microwave-assisted synthesis. Different from the rapid thermal energy input of microwave fields, laser-assisted synthesis from the perspective of microenvironment engineering realizes transient extreme energy input and ultrafast quenching *via* light–matter interactions.[111] It creates extreme temperature and pressure environments at the microscale, enabling the preparation of metastable phases and single-atom/diatom structures that are inaccessible through traditional thermodynamic pathways. This opens a new route for the controllable synthesis of high-performance materials for catalysis, energy conversion, and related applications.

Laser solid-phase synthesis demonstrates multidimensional core advantages in material preparation by leveraging the unique energy characteristics of lasers. Liu *et al.* utilized a UV laser to simultaneously reduce metal precursors and organic compounds, combining photothermal and photochemical effects to achieve one-step laser synthesis of dual-atom alloy catalysts (Fig. 12a).[112] In this study, the UV laser (355 nm) regulated the synthesis microenvironment through photochemical–photothermal synergy: the photochemical effect, with its 3.5 eV photon energy, could break Pt–Cl (3.47 eV) and C–H (2.55 eV) bonds while preserving C–C bonds (6.11 eV), enabling defects to be selectively generated only on the surface of Co nanoparticles (Co vacancy formation energy 1.25 eV, low) as anchor sites for Pt–Ru dual atoms, while simultaneously directly reducing $Pt^{4+}$ and $Ru^{3+}$ to lower their oxidation states; the photothermal effect generated a mild temperature of 375 °C (cooling rate $1.2 \times 10^4$ °C $s^{-1}$), enabling synchronous reduction of metal precursors and carbonization of ZIF-67@PBI into low-defect graphene, avoiding structural damage caused by high temperatures. The synthesis mechanism involves one-step laser conversion: first, $H_2PtCl_6$, $(NH_4)_2RuCl_6$, ZIF-67, and PBI are mixed to form a (Pt–Ru)/ZIF-67@PBI precursor film; subsequently, the UV laser irradiates the precursor, where the photochemical effect reduces and releases low oxidation state Pt/Ru active species, and the photothermal effect carbonizes ZIF-67@PBI, reduces $Co^{2+}$ to Co nanoparticles while generating surface defects; the Pt/Ru active species preferentially anchor at the Co defect sites to form Pt–Ru dual-atom pairs, with electron transfer from Co to Pt/Ru enhancing the interaction, ultimately yielding the UV-$(PtRu)_1$Co dual-atom alloy catalyst supported on low-defect graphene (alloy particle size ≈3.1 nm) (Fig. 12b–d).

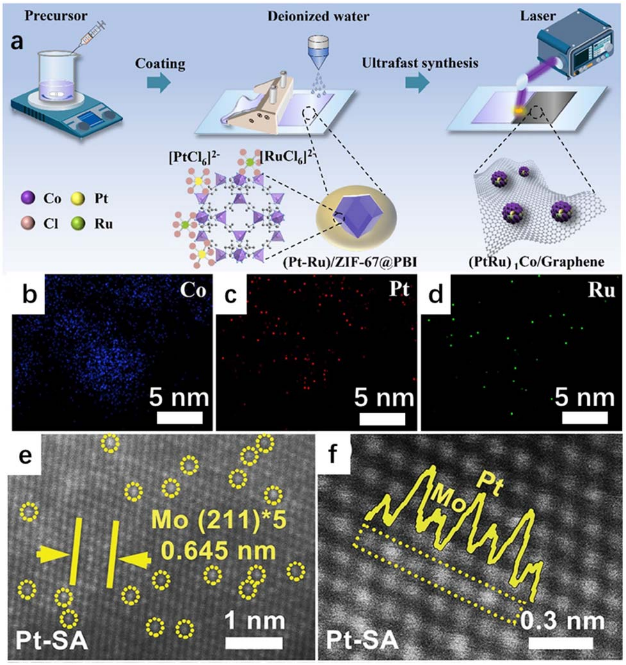

Fig. 12 (a) Schematic illustration of the laser synthesis of $(PtRu)_1$Co/graphene. (b–d) EDS results of UV-$(PtRu)_1$Co DAAs. (e and f) Atomic-resolution HAADF-STEM image of Mo (211) for Pt-SA/Mo-L. Pt single atoms are marked by yellow circles. The yellow curve represents the integrated pixel intensity in the yellow dotted box.

The Laser Liquid Ablation (LAL) strategy provides a promising pathway for the synthesis of single-atom alloy electrodes. Laser energy is absorbed and converted into thermal energy, generating extremely high temperatures within femtoliter volumes at the target material. Due to the localized high-temperature characteristics of the laser, precursors such as metal ions or compounds on the target material surface undergo rapid thermal decomposition, and the highly active plasma interacts with the solvent or ions to synthesize nanomaterials. Zhou *et al.* achieved precise regulation of the synthesis microenvironment through a nanosecond laser ablation strategy.[113] On the one hand, energy is focused within a femtoliter volume, instantaneously generating a local temperature of ≈2000 K (reaching 1000 °C within 4 seconds), providing the activation energy for the thermal decomposition of the Pt–O–Mo precursor, while leveraging the solution environment to achieve ultra-fast cooling (cooling rate up to $10^7$ °C $s^{-1}$), thermodynamically suppressing the aggregation of Pt atoms. On the other hand, the laser irradiation process generates $H_2$ reducing gas within the solution, creating a local reducing atmosphere. This regulation method is versatile, enabling the dispersion of noble metals such as Pt, Rh, Ir, and Ru as single atoms on the surface of Mo foil. The synthesis mechanism involves a two-step process: first, a piece of clean Mo foil is immersed in a 0.2 mmol $L^{-1}$ $H_2PtCl_6$ solution, forming a Pt–O–Mo/Mo precursor *via* the redox reaction between $Pt^{4+}$ and $Mo^0$ (Pt, Mo, and O are uniformly distributed, with no Pt crystalline phase). Subsequently, laser irradiation of the precursor decomposes the Pt–O–Mo bonds *via* localized high temperature, releasing Pt active species. The ultra-fast cooling forces the selective embedding of Pt single atoms into the (211) crystal plane of Mo, while the $H_2$ reduces the Pt active species to $Pt^0$ and facilitates the formation of strong Pt–Mo bonds, ultimately yielding a self-supporting Pt-SA/Mo-L single-atom alloy electrode (Fig. 12e and f).

In summary, laser-assisted synthesis has transcended the scope of merely replacing traditional methods and is progressively evolving into a materials creation platform capable of innovating new structures, discovering new mechanisms, and expanding new functionalities.[114] This technology endows researchers with the unique capability to precisely manipulate atomic arrangement and electronic structure under non-equilibrium conditions, providing a novel pathway for the directional design of high-performance, cross-scale functional materials. In the future, with the deep integration of ultrafast spectroscopy, *in situ* characterization, and theoretical simulation, the mechanisms of laser synthesis processes will be more systematically revealed. Combined with automated control and artificial intelligence technologies, it is expected to achieve full-chain intelligent manufacturing from material design and synthesis to performance optimization, propelling innovative applications of nanomaterials in critical fields such as energy, environment, and information into a new stage.

### 4.3 Magnetic field-assisted synthesis technology

As a non-thermal energy strategy for external energy environment regulation, magnetic field-assisted synthesis modulates the microreaction field *via* a non-contact external energy field.[115] Different from the thermal energy input modes of microwaves and lasers, magnetic field-assisted synthesis from the perspective of microenvironment engineering relies on magnetic forces and magnetohydrodynamic effects as the core mechanisms. It achieves non-thermal control of particle directional assembly and ion mass transfer, with the advantages of high regulation precision and wide material applicability.

Yang *et al.* employed a magnetic field-assisted gelation method to regulate the microenvironment.[116] The magnetic field induces magnetization of Ni nanoparticles, causing them to directionally aggregate along the field lines, while synergizing with the buoyancy of $N_2$ bubbles generated by the reaction to drive the migration of Ni nanochains toward the surface of the reaction solution. This establishes a nanochain concentration gradient with high concentration at the surface and low concentration at the bottom. Additionally, the magnetic field accelerates cold welding between nanowires, forming numerous metal–metal bonds that strengthen interfacial bonding. This enables the gel network to withstand capillary forces during air drying and induces the formation of an anisotropic structure characterized by "random in-plane distribution and layered out-of-plane ordering" (Fig. 13a). The synthesis mechanism is as follows: Using $NiCl_2$ as the nickel source and hydrazine as the reducing agent under a 300 Gs magnetic field, magnetized Ni nanoparticles are first generated *via* a reduction reaction. These nanoparticles directionally assemble into nanochains along the magnetic field and migrate to the surface until reaching the critical concentration for gelation. Subsequently, the surface nanochains form a gel layer through van der Waals forces and magnetic interactions, while the underlying nanochains continuously supplement and undergo cold welding and cross-linking with the upper layer to form a thick gel. Finally, air drying yields a low-density, highly compressible NNWA.

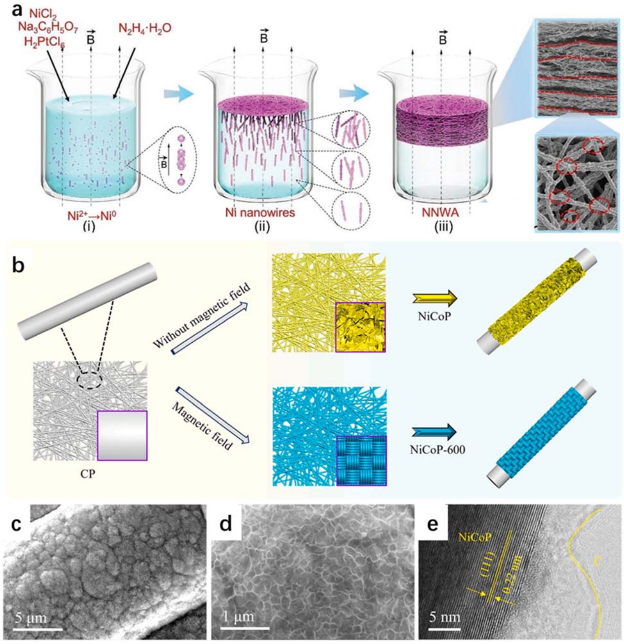

Fig. 13 (a) NNWAs during different preparation stages. Schematic diagram of the magnetic field-assisted preparation process of the NNWAs. (b) The schematic for the preparation of NiCoP and NiCoP-600 on carbon paper. (c and d) SEM and (e) HRTEM images of NiCoP.

Unlike its primary reliance on magnetization forces for guiding assembly in gel systems, magnetic fields play a crucial role in electrochemical deposition processes mainly through magnetohydrodynamic effects. Wang's study exemplifies the regulation of microenvironment and synthesis processes *via* magnetic electrodeposition (Fig. 13b).[117] Based on the magnetohydrodynamic effect, the magnetic field thins the ion diffusion layer on the electrode surface to enhance ion transport, accelerates the preferential deposition of $Co^{2+}$ to optimize the Ni/Co ratio, suppresses bubble agglomeration on the electrode surface and improves material wettability. Simultaneously, it guides charged particles ($Ni^{2+}$, $Co^{2+}$, and $H_2PO_2^-$) to deposit along the electrode convex surface and surrounding areas, avoiding the loose flower-like structure formed without a magnetic field and resulting in a dense braided-rope structure. The synthesis mechanism is as follows: using hydrophilic carbon paper as the substrate, $NiCl_2/CoCl_2$ as metal sources, and $NaH_2PO_2$ as the phosphorus source, a three-electrode system is constructed under a 600 mT magnetic field. Constant potential electrodeposition at −1 V is performed, where the MHD effect drives directional ion transport and spiral particle deposition. $Co^{2+}$ is preferentially deposited and forms NiCoP *in situ* with Ni and P, ultimately yielding dense braided-rope-like NiCoP with high specific surface area and high HER activity (Fig. 13c–e).

In summary, as an efficient and green non-contact physical field regulation strategy, the core advantage of magnetic field-assisted synthesis technology lies in its ability to profoundly influence the synthesis microenvironment through different physical mechanisms, thereby achieving precise construction of materials from microstructure to macroscopic performance.[118] It breaks through the limitations of traditional synthesis methods in terms of regulation dimensions and precision, not only providing new solutions for performance optimization of existing material systems but also opening broad prospects for promoting the innovative design and controllable preparation of future high-end functional materials.

### 4.4 Ultrasound-assisted synthesis technology

As a multi-effect synergistic strategy for external energy environment regulation, ultrasound-assisted synthesis relies on non-contact external energy fields to modulate the micro-reaction field.[119] Different from the single physical field effect of magnetic fields, ultrasound-assisted synthesis from the perspective of microenvironment engineering is centered on the ultrasonic cavitation effect. It achieves simultaneous synergy of thermal, mechanical, and flow field effects at the microscale, with multiple functions including exfoliation, dispersion, and reaction promotion, making it a green and efficient microenvironment regulation approach.

These unique advantages enable ultrasound technology to demonstrate exceptional capabilities in the controlled synthesis of various nanomaterials. Ultrasound plays a dual role in microenvironment regulation for both BP nanosheets and CSS@BP composite materials (Fig. 14a). When preparing BP nanosheets, Wang's research team utilized ultrasound to regulate size and layer thickness: mechanical force exfoliation of bulk BP through ultrasonication yielded thin-layer nanosheets approximately 200 nm in size, while performing ultrasonication in an ice-water bath suppressed oxidative degradation of BP caused by ultrasound-induced heating, maintaining its chemical stability.[120] In preparing CSS@BP composites, ultrasound regulated microscopic distribution: it broke up CSS particle aggregates, enabling their uniform dispersion and attachment onto BP nanosheet surfaces, forming an ordered structure mimicking chloroplasts. Simultaneously, ultrasound promoted intimate interfacial contact between CSS and BP, providing sufficient interaction sites for photothermal performance synergy. During BP nanosheet preparation, the transient high pressure and shear forces generated by ultrasonic cavitation disrupted weak van der Waals forces between bulk BP layers, achieving liquid-phase exfoliation, while ethanol solvation layers combined with continuous ultrasonication prevented nanosheet aggregation, and the ice-water bath inhibited BP oxidation. During CSS@BP composite preparation, ultrasonic shear forces fragmented CSS aggregates, enabling their uniform adsorption in the BP nanosheet dispersion, and ultrasound-promoted intimate interfacial contact, ensured composite structural stability, and ultimately yielded a chloroplast-like composite material with a "BP framework–CSS particle" structure.

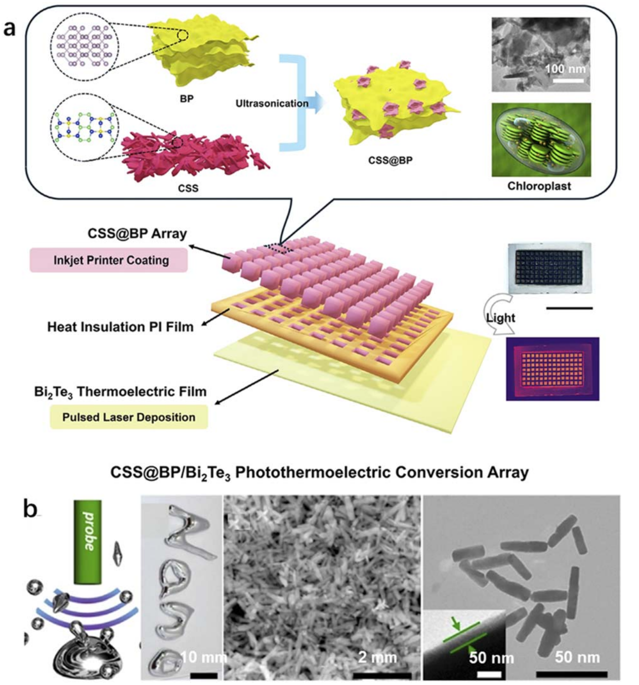

Fig. 14 (a) CSS@BP/$Bi_2Te_3$ photo thermoelectric conversion array: schematic and physical representation of the array structure. (b) Fabrication of EGaIn colloidal motors through an acoustically assisted physical dispersion and SEM images of EGaIn colloidal motors.

He's research demonstrates the critical role of ultrasound in microenvironment regulation during the synthesis of EGaIn liquid metal colloidal nanorods.[121] Ultrasound achieves triple regulatory effects: it disrupts the surface tension-induced aggregation tendency of EGaIn liquid metal to ensure monodispersity of nanoparticles; utilizes continuous ultrasonic shear forces to "stretch" liquid metal microdroplets into uniform rod-like structures (210 nm diameter, 850 nm length, ∼4 aspect ratio) rather than random spheres; and promotes uniform oxygen diffusion to the EGaIn droplet surface, enabling selective oxidation of the more reactive Ga atoms to form a homogeneous ∼30 nm thick GaOOH shell while preventing localized uneven oxidation. The synthesis mechanism relies on the synergistic effect of ultrasonic cavitation and shear forces: ultrasound generates formation, oscillation, and collapse of cavitation bubbles in the water–ethanol system, releasing transient high pressure and shear forces that break the continuous EGaIn phase into nanoscale droplets, with continuous shear further stretching them into rods. Simultaneously, ultrasound-enhanced oxygen diffusion facilitates preferential surface oxidation of Ga to GaOOH, ultimately forming core–shell structured nanorods with a "liquid EGaIn core–solid GaOOH shell" configuration (Fig. 14b).

In summary, as a multi-effect synergistic strategy for external energy environment regulation, ultrasound-assisted synthesis is uniquely characterized by achieving synergistic regulation of microscale thermal, mechanical, and flow fields *via* the cavitation effect. It combines multiple functions with the advantages of being green and efficient, making it the most comprehensive non-contact regulation strategy in external energy environment control. Together with the aforementioned thermal energy and non-thermal physical field strategies, it forms a complete system for external energy environment regulation.[121]

## 5 Outlook

Looking ahead, research on microenvironment regulation in nanomaterial synthesis will undergo profound paradigm shifts and technological innovations in both fundamental scientific understanding and industrial application. Whether in local physicochemical environments, spatial confinement effects, or external energy environments, the regulatory essence lies in precisely manipulating nucleation and growth of materials by reconstructing the thermodynamic and kinetic conditions of the reaction microzone. The core of the next stage in this field is to integrate dispersed regulation strategies into a systematic design theory across multiple dimensions, which also serves as the key focus of this review.[29]

At the fundamental research level, the current core bottleneck is the lack of in-depth atomic/molecular-scale understanding of the dynamic processes and multi-dimensional coupling mechanisms in microenvironment regulation. Single-dimensional mechanistic analysis can no longer meet the demands of precise design, and the absence of dynamic quantitative models for cross-dimensional coupling constitutes the key reason for the remaining "black box" in regulation. The systematic summary of three-dimensional regulation strategies, in-depth analysis of structure–activity relationships, and comparative investigation of common characteristics presented in this review provide an essential research framework and starting point to break through this bottleneck and clarify the key directions and core targets for cross-dimensional coupling studies. Most existing studies conduct static and isolated analyses of single environmental factors, which can hardly reproduce the complex dynamic scenarios of multi-field coupling. In addition, the microscopic mechanisms of energy transfer–structure transformation in external energy environments remain unclear, severely restricting the rational design of intelligent nanomaterials. To address these challenges, future fundamental research will achieve a leap from qualitative observation to quantitative programming. Based on accumulated research progress, we propose two core directions: first, develop *in situ* real-time characterization techniques with multi-field coupling and multi-scale linkage. Relying on the dimensional coupling relationships identified in this review, dynamically resolve the interaction rules among microenvironment dimensions and their correlation with the evolution of material structures, thus fundamentally unlocking the mechanistic "black box". Second, deeply integrate artificial intelligence and multi-scale theoretical calculations. Establish a dedicated database based on the three-dimensional regulation features summarized in this review, and build a research paradigm combining data-driven approaches and theoretical simulations, so as to realize the inverse design of optimal microenvironment conditions and on-demand customization of nanomaterial properties.[122–125]

Regarding industrial translation, microenvironment regulation technologies still face three core challenges: poor consistency in large-scale production, insufficient cost-effectiveness and sustainability, and low material stability under real working conditions.[126,127] The three-dimensional regulation principles, common characteristics, and differentiated advantages of each strategy summarized in this review provide important theoretical references and technical insights to address these industrial pain points and outline feasible pathways for the engineering implementation of microenvironment regulation. To tackle the above issues, we propose targeted development strategies: first, in response to the "scale-up effect", and based on the microscale regulation principles outlined in this review, develop continuous and modular manufacturing processes for microenvironments to accurately reproduce microscale regulation conditions in industrial macroscale systems, thus fundamentally ensuring product quality stability. Second, for cost and environmental concerns, relying on the green regulation strategies summarized herein, focus on promoting technologies such as biomass-based templates and low-energy external field coupling, combined with green and low-cost raw material systems, to solve the economic and environmental issues of industrialization at the source. Third, to improve stability under service conditions, integrated with the microenvironment design logic of this review, establish a high-fidelity testing platform that combines synthesis and service microenvironments to realize the full-life-cycle design of materials *via* microenvironment regulation, significantly enhancing the robustness of materials in practical applications. Ultimately, by integrating intelligent perception and adaptive control algorithms, a smart factory capable of real-time regulation of three-dimensional microenvironment parameters will be constructed, promoting the large-scale and intelligent manufacturing of high-performance nanomaterials.[128]

The deep integration of the data-driven and theoretical simulation research paradigm will completely break through the efficiency bottleneck of the traditional trial-and-error approach. Meanwhile, the three-dimensional regulation framework established in this review provides a clear parameter system and research boundary for the implementation of this paradigm. In the future, first-principles calculations will be used to clarify the intrinsic mechanisms of microenvironment regulation based on the dimensional classification in this work, and to establish an accurate quantitative mapping from regulation parameters to material structures. With the aid of machine learning, the synthetic parameter space can be rapidly optimized, and the construction of adaptive microreaction systems will be empowered. This will enable full-dimensional dynamic monitoring of key microenvironmental variables inside the reactor and intelligent coordination of cross-dimensional regulation. This will fundamentally guarantee the consistency and scale-up potential of nanomaterial synthesis and ultimately drive the field of nanomaterial synthesis into a new era of intelligence, digitization, and programmability. On-demand design of nanomaterials *via* microenvironment engineering will thus become a reality.[129]

## Author contributions

L. W. and J. L. supervised the research. J. L. conceived the research. S. P. collected documents, sorted out materials, and wrote the original manuscript. Y. L., X. X., K. S, H. L., and J. C. helped supervision, writing – review & editing. All authors discussed the results and commented on the manuscript.

## Conflicts of interest

There are no conflicts to declare.

## Data availability

No primary research results, software or code have been included and no new data were generated or analysed as part of this review.

## Acknowledgements

This work was supported by the National Natural Science Foundation of China (52272222), Taishan Scholar Young Talent Program (tsqn201909114 and tsqn201909123), and University Youth Innovation Team of Shandong Province (202201010318).

## References

1 W. T. Grubb, *Nature*, 1963, **198**, 883–884.
2 J. Zhou, A. I. Chizhik, S. Chu and D. Jin, *Nature*, 2020, **579**, 41–50.
3 J. C. Crocker, *Nature*, 2008, **451**, 528–529.
4 N. Kittner, F. Lill and D. M. Kammen, *Nat. Energy*, 2017, **2**, 17125.
5 W. Li, J. Liu and D. Zhao, *Nat. Rev. Mater.*, 2016, **1**, 16023.
6 M. Zhao, K. Yuan, Y. Wang, G. Li, J. Guo, L. Gu, W. Hu, H. Zhao and Z. Tang, *Nature*, 2016, **539**, 76–80.
7 H. Li, J. Lai, Z. Li and L. Wang, *Adv. Funct. Mater.*, 2021, **31**, 2106715.
8 D. Zhang, H. Zhao, X. Wu, Y. Deng, Z. Wang, Y. Han, H. Li, Y. Shi, X. Chen, S. Li, J. Lai, B. Huang and L. Wang, *Adv. Funct. Mater.*, 2021, **31**, 2006939.
9 Z. Pei, H. Lei and L. Cheng, *Chem. Soc. Rev.*, 2023, **52**, 2031–2081.
10 W. Park, H. Shin, B. Choi, W.-K. Rhim, K. Na and D. Keun Han, *Prog. Mater. Sci.*, 2020, **114**, 100686.
11 T. Domröse, T. Danz, S. F. Schaible, K. Rossnagel, S. V. Yalunin and C. Ropers, *Nat. Mater.*, 2023, **22**, 1345–1351.
12 T. Chlouba, R. Shiloh, S. Kraus, L. Brückner, J. Litzel and P. Hommelhoff, *Nature*, 2023, **622**, 476–480.
13 L. Chen, R. Luque and Y. Li, *Chem. Soc. Rev.*, 2017, **46**, 4614–4630.
14 M.-C. Li, X. Liu, K. Lv, J. Sun, C. Dai, B. Liao, C. Liu, C. Mei, Q. Wu and M. Hubbe, *Prog. Mater. Sci.*, 2023, **139**, 101187.
15 K. R. Ryan, M. P. Down, N. J. Hurst, E. M. Keefe and C. E. Banks, *eScience*, 2022, **2**, 365–381.
16 K. A. Darling, M. Rajagopalan, M. Komarasamy, M. A. Bhatia, B. C. Hornbuckle, R. S. Mishra and K. N. Solanki, *Nature*, 2016, **537**, 378–381.
17 P. J. Santos, P. A. Gabrys, L. Z. Zornberg, M. S. Lee and R. J. Macfarlane, *Nature*, 2021, **591**, 586–591.
18 J. Zhang, Z. Chen, Q. Ai, T. Terlier, F. Hao, Y. Liang, H. Guo, J. Lou and Y. Yao, *Joule*, 2021, **5**, 1845–1859.
19 Y. Xia, *Nat. Mater.*, 2008, **7**, 758–760.
20 J. Ma and X. Yin, *Science*, 2025, **387**, eadw1922.
21 M. Zhang, Y. Lai, M. Li, T. Hong, W. Wang, H. Yu, L. Li, Q. Zhou, Y. Ke, X. Zhan, T. Zhu, C. Huang and P. Yin, *Angew. Chem., Int. Ed.*, 2019, **58**, 17412–17417.
22 D. Kim, M. Kim, S. Reidt, H. Han, A. Baghizadeh, P. Zeng, H. Choi, J. Puigmartí-Luis, M. Trassin, B. J. Nelson, X.-Z. Chen and S. Pané, *Nat. Commun.*, 2023, **14**, 750.
23 D. T. Yimam, M. Liang, J. Ye and B. J. Kooi, *Adv. Mater.*, 2024, **36**, 2303502.
24 L. Gao, Y. Liu, J. Su, K. Liu and H. Zhang, *Adv. Mater.*, 2025, **37**, 2419349.
25 X. Wang, J. Feng, Y. Bai, Q. Zhang and Y. Yin, *Chem. Rev.*, 2016, **116**, 10983–11060.
26 S. Zhang, X. Liu, C. Jia, Z. Sun, H. Jiang, Z. Jia and G. Wu, *Nano-Micro Lett.*, 2023, **15**, 204.
27 J. Wu, X. Bai, L. Yan, D. Baimanov, Y. Cong, P. Quan, R. Cai, Y. Guan, W. Bu, B. Lin, J. Wang, S. Yu, S. Li, Y. Chong, Y. Li, G. Hu, Y. Zhao, C. Chen and L. Wang, *Nat. Commun.*, 2024, **15**, 8349.
28 M. Liu, M. Yang, X. Wan, Z. Tang, L. Jiang and S. Wang, *Adv. Mater.*, 2023, **35**, 2208995.
29 Z.-S. Zhu, S. Zhong, C. Cheng, H. Zhou, H. Sun, X. Duan and S. Wang, *Chem. Rev.*, 2024, **124**, 11348–11434.
30 H. Sun, L. Mei, J. Liang, Z. Zhao, C. Lee, H. Fei, M. Ding, J. Lau, M. Li, C. Wang, X. Xu, G. Hao, B. Papandrea, I. Shakir, B. Dunn, Y. Huang and X. Duan, *Science*, 2017, **356**, 599–604.
31 M. H. Oh, M. G. Cho, D. Y. Chung, I. Park, Y. P. Kwon, C. Ophus, D. Kim, M. G. Kim, B. Jeong, X. W. Gu, J. Jo, J. M. Yoo, J. Hong, S. McMains, K. Kang, Y.-E. Sung, A. P. Alivisatos and T. Hyeon, *Nature*, 2020, **577**, 359–363.
32 R. Zhang, S. Zhao, J. Ding, Y. Chong, T. Jia, C. Ophus, M. Asta, R. O. Ritchie and A. M. Minor, *Nature*, 2020, **581**, 283–287.
33 M.-L. Gao, L. Li, Z.-X. Sun, J.-R. Li and H.-L. Jiang, *Angew. Chem., Int. Ed.*, 2022, **61**, e202211216.
34 J. Qu, Y. Wang, X. Mu, J. Hu, B. Zeng, Y. Lu, M. Sui, R. Li and C. Li, *Adv. Mater.*, 2022, **34**, 2203320.

35 V. Muravev, A. Parastaev, Y. van den Bosch, B. Ligt, N. Claes, S. Bals, N. Kosinov and E. J. M. Hensen, *Science*, 2023, **380**, 1174–1179.

36 J. Wang, C. Cheng, X. Zheng, J. C. Idrobo, A.-Y. Lu, J.-H. Park, B. G. Shin, S. J. Jung, T. Zhang, H. Wang, G. Gao, B. Shin, X. Jin, L. Ju, Y. Han, L.-J. Li, R. Karnik and J. Kong, *Nature*, 2023, **623**, 956–963.

37 H.-F. Geng, Y.-F. Bao, X. Wang and B. Ren, *Nat. Catal.*, 2025, **8**, 753–754.

38 H. Li, Y. Han, H. Zhao, W. Qi, D. Zhang, Y. Yu, W. Cai, S. Li, J. Lai, B. Huang and L. Wang, *Nat. Commun.*, 2020, **11**, 5437.

39 Z. Wang, Z. Yi, L. W. Wong, X. Tang, H. Wang, H. Wang, C. Zhou, Y. He, W. Xiong, G. Wang, G. Zeng, J. Zhao and P. Xu, *Adv. Mater.*, 2024, **36**, 2404278.

40 Y. Zhang, F. Liu, M. Yang, H. Xin, B. Wu, J. J. Li, H. Tao, Y. Chen, J. Chen, Q. Guan, Z. Liu, Z. Xu, J. Pei, S. Moya, H. Pan, X. Zhao, L. Kong and G. Wang, *Adv. Mater.*, 2025, **37**, 2502741.

41 Y. Lian, Y. Wang, Y. Yuan, Z. Ren, W. Tang, Z. Liu, S. Xing, K. Ji, B. Yuan, Y. Yang, Y. Gao, S. Zhang, K. Zhou, G. Zhang, S. D. Stranks, B. Zhao and D. Di, *Nature*, 2025, **640**, 62–68.

42 C. Kim, S. O. Park, S. K. Kwak, Z. Xia, G. Kim and L. Dai, *Nat. Commun.*, 2023, **14**, 5822.

43 W. Li, L. Li, Z. Liu, S. Zheng, Q. Li and F. Yan, *Adv. Mater.*, 2023, **35**, 2301383.

44 M. Dindo, A. Bevilacqua, G. Soligo, V. Calabrese, A. Monti, A. Q. Shen, M. E. Rosti and P. Laurino, *J. Am. Chem. Soc.*, 2024, **146**, 15965–15976.

45 A. Nie, Z. Zhao, B. Xu and Y. Tian, *Nat. Mater.*, 2025, **24**, 1172–1185.

46 L. Jiang, L. Jiang, X. Luo, R. Li, Q. Zhou, W. Zeng, J. Yu, L. Chen and S. Mu, *eScience*, 2025, **5**, 100398.

47 A. Teixeira do Nascimento, P. R. Stoddart, T. Goris, M. Kael, R. Manasseh, K. Alt, J. Tashkandi, B. C. Kim and S. E. Moulton, *Adv. Mater.*, 2025, **37**, e07559.

48 C. Xiao, M. Liu, K. Yao, Y. Zhang, M. Zhang, M. Yan, Y. Sun, X. Liu, X. Cui, T. Fan, C. Zhao, W. Hua, Y. Ying, Y. Zheng, D. Zhang, C.-W. Qiu and H. Zhou, *Nature*, 2025, **643**, 80–88.

49 L.-L. Xu, C.-F. Wang and S. Chen, *Angew. Chem., Int. Ed.*, 2014, **53**, 3988–3992.

50 A. Pal, V. Malik, L. He, B. H. Erné, Y. Yin, W. K. Kegel and A. V. Petukhov, *Angew. Chem., Int. Ed.*, 2015, **54**, 1803–1807.

51 F. G. Baddour, C. P. Nash, J. A. Schaidle and D. A. Ruddy, *Angew. Chem., Int. Ed.*, 2016, **55**, 9026–9029.

52 B. Pieber, M. Shalom, M. Antonietti, P. H. Seeberger and K. Gilmore, *Angew. Chem., Int. Ed.*, 2018, **57**, 9976–9979.

53 Z. Zheng, X. Shang, W. Wang, X. Yang, X. Su and Y. Huang, *Angew. Chem., Int. Ed.*, 2025, **64**, e202422953.

54 H. Li, M. Sun, Y. Pan, J. Xiong, H. Du, Y. Yu, S. Feng, Z. Li, J. Lai, B. Huang and L. Wang, *Appl. Catal., B*, 2022, **312**, 121431.

55 P. Energy Storage Mater.Zhou, L. Zhang, Y. Liu, Q. Zhou, J. Zheng, X. Zhang, X. Fan, X. Xiao and L. Chen, *Energy Storage Mater.*, 2025, **82**, 104562.

56 Z. Lv, S. Zhou, L. Zhao, Z. Liu, J. Liu, W. Xu, L. Wang and J. Lai, *Adv. Energy Mater.*, 2023, **13**, 2300946.

57 L. Zhao, Z. Lv, Y. Shi, S. Zhou, Y. Liu, J. Han, Q. Zhang, J. Lai and L. Wang, *Energy Environ. Sci.*, 2024, **17**, 1291.

58 F. Liu, J. Zhou, X. Gao, R. Shi, Z. Guo, E. C. M. Tse and Y. Chen, *Angew. Chem., Int. Ed.*, 2025, **64**, e202422183.

59 X. Liu, J. Luo, H. Wang, L. Huang, S. Wang, S. Li, Z. Sun, F. Sun, Z. Jiang, S. Wei, W.-X. Li and J. Lu, *Angew. Chem., Int. Ed.*, 2022, **61**, e202202330.

60 P. Tang, S. Guan, C. Wu, H. Wu, N. Lu, J. Tan, C. Wang, H.-M. Cheng and F. Li, *Angew. Chem., Int. Ed.*, 2025, **64**, e202503108.

61 J. Shi, K. Sun, Z. Chen, Y. Qiu, H. Liu, W. Ma, Q. Liu and Z. Ge, *Angew. Chem., Int. Ed.*, 2024, **63**, e202318360.

62 D. Fan, X. Chen, S. Wang, J. Zhan, Y. Chen, H. Zhou, D. Li, H. Tang, Q. He and T. Chen, *Angew. Chem., Int. Ed.*, 2025, **64**, e202423799.

63 W. J. Stark, P. R. Stoessel, W. Wohlleben and A. Hafner, *Chem. Soc. Rev.*, 2015, **44**, 5793–5805.

64 Z. Wang, Z. Yang, Z. C. Kadirova, M. Guo, R. Fang, J. He, Y. Yan and J. Ran, *Coord. Chem. Rev.*, 2022, **473**, 214794.

65 Y. Qu, L. Wang, Z. Li, P. Li, Q. Zhang, Y. Lin, F. Zhou, H. Wang, Z. Yang, Y. Hu, M. Zhu, X. Zhao, X. Han, C. Wang, Q. Xu, L. Gu, J. Luo, L. Zheng and Y. Wu, *Adv. Mater.*, 2019, **31**, 1904496.

66 J. Li, Y. Huang, J. Huang, G. Liang, Y. Zhang, G. Rey, F. Guo, Z. Su, H. Zhu, L. Cai, K. Sun, Y. Sun, F. Liu, S. Chen, X. Hao, Y. Mai and M. A. Green, *Adv. Mater.*, 2020, **32**, 2005268.

67 Y. Yuan, T. Wang, H. Chen, S. M. Mahurin, H. Luo, G. M. Veith, Z. Yang and S. Dai, *Angew. Chem., Int. Ed.*, 2020, **59**, 21935–21939.

68 C. Hu, S. Tu, N. Tian, T. Ma, Y. Zhang and H. Huang, *Angew. Chem., Int. Ed.*, 2021, **60**, 16309–16328.

69 Z. Li, M. Chen, Z. Chen, Y.-L. Zhu, C. Guo, H. Wang, Y. Qin, F. Fang, D. Wang, C. Su, C. He, X. Yu, Z.-Y. Lu and X. Li, *J. Am. Chem. Soc.*, 2022, **144**, 22651–22661.

70 N. Bui, E. R. Meshot, S. Kim, J. Peña, P. W. Gibson, K. J. Wu and F. Fornasiero, *Adv. Mater.*, 2016, **28**, 5871–5877.

71 B. Qin, J. Jiang, L. Wang, Q. Guo, C. Zhang, L. Xu, X. Ni, P. Yin, L.-M. Peng, E. Wang, F. Ding, C. Qiu, C. Liu and K. Liu, *Science*, 2025, **389**, 299–302.

72 Q. Cheng, T. Wang, Y. Chen, Y. Pan, Y. Chen, B. Yang and H. Yang, *eScience*, 2025, **6**, 100453.

73 H. Li, X. Qian, H. Mohanram, X. Han, H. Qi, G. Zou, F. Yuan, A. Miserez, T. Liu, Q. Yang, H. Gao and J. Yu, *Nat. Nanotechnol.*, 2024, **19**, 1141–1149.

74 B. Yu, J. Duan, H. Cong, W. Xie, R. Liu, X. Zhuang, H. Wang, B. Qi, M. Xu, Z. L. Wang and J. Zhou, *Science*, 2020, **370**, 342–346.

75 T. Liu, L. Yu, J. Lu, T. Zhou, X. Huang, Z. Cai, A. Dai, J. Gim, Y. Ren, X. Xiao, M. V. Holt, Y. S. Chu, I. Arslan, J. Wen and K. Amine, *Nat. Commun.*, 2021, **12**, 6024.

76 Z. Zhang, P. Yu, Z. Liu, K. Liu, Z. Mu, Z. Wen, J. She, Y. Bai, Q. Zhang, T. Cheng and C. Gao, *J. Am. Chem. Soc.*, 2025, **147**, 9640–9652.

77 P. Liu, X. Zhang, J. Fei, Y. Shi, J. Zhu, D. Zhang, L. Zhao, L. Wang and J. Lai, *Adv. Mater.*, 2024, **36**, 2310591.

78 S. Dou, Y. Shao, L. Fan, D. Zhang, J. Xu, J. Zhang, H. Tian, Y.-B. He, C. Mao, H. Zhu, W. Gan, J. Zeng, W.-D. Liu,

J. Zhou, Y. Chen and Q. Yuan, *Adv. Funct. Mater.*, 2025, **35**, 2412551.
79 J. C. Ondry, Z. Zhou, K. Lin, A. Gupta, J. H. Chang, H. Wu, A. Jeong, B. F. Hammel, D. Wang, H. C. Fry, S. Yazdi, G. Dukovic, R. D. Schaller, E. Rabani and D. V. Talapin, *Science*, 2024, **386**, 401–407.
80 Z. Zhou, J. C. Ondry, Y.-C. Liu, H. Wu, A. Jeong, A. Gupta, Y.-C. Chen, J. H. Chang, R. D. Schaller and D. V. Talapin, *J. Am. Chem. Soc.*, 2025, **147**, 9198–9209.
81 V. Kamysbayev, A. S. Filatov, H. Hu, X. Rui, F. Lagunas, D. Wang, R. F. Klie and D. V. Talapin, *Science*, 2020, **369**, 979–983.
82 W. Guo, G. Zhao, Z. Huang, Z. Luo, X. Zheng, M. Gao, Y. Liu, H. Pan and W. Sun, *Angew. Chem., Int. Ed.*, 2025, **64**, e202414516.
83 J. Tang, N. Meftahi, A. J. Christofferson, J. Sun, R. Yu, M. A. Rahim, J. Tang, G. Mao, T. Daeneke, R. B. Kaner, S. P. Russo and K. Kalantar-Zadeh, *Nat. Commun.*, 2025, **16**, 907.
84 H. Zhang, Y. Wang, X. Liu, F. Wu, X. Wang, C. Ma, X. Han, Y. Ran, Y. Zhang, Z. Zhang, Q. Xu, Z. Wang, G. Zhang, J. Wang, J. Cai, Z. Liu, Y. Zhang, T. Yao, J. Jiang and Y. Wu, *Angew. Chem., Int. Ed.*, 2025, **64**, e202421554.
85 S. A. Idrus-Saidi, J. Tang, S. Lambie, J. Han, M. Mayyas, M. B. Ghasemian, F.-M. Allioux, S. Cai, P. Koshy, P. Mostaghimi, K. G. Steenbergen, A. S. Barnard, T. Daeneke, N. Gaston and K. Kalantar-Zadeh, *Science*, 2022, **378**, 1118–1124.
86 A. Zavabeti, J. Z. Ou, B. J. Carey, N. Syed, R. Orrell-Trigg, E. L. H. Mayes, C. Xu, O. Kavehei, A. P. O'Mullane, R. B. Kaner, K. Kalantar-zadeh and T. Daeneke, *Science*, 2017, **358**, 332–335.
87 J. Tang, A. J. Christofferson, J. Sun, Q. Zhai, P. V. Kumar, J. A. Yuwono, M. Tajik, N. Meftahi, J. Tang, L. Dai, G. Mao, S. P. Russo, R. B. Kaner, M. A. Rahim and K. Kalantar-Zadeh, *Nat. Nanotechnol.*, 2024, **19**, 306–310.
88 B.-C. Ye, W.-H. Li, X. Zhang, J. Chen, Y. Gao, D. Wang and H. Pan, *Adv. Mater.*, 2024, **36**, 2402747.
89 M. P. Hendricks, M. P. Campos, G. T. Cleveland, I. Jen-La Plante and J. S. Owen, *Science*, 2015, **348**, 1226–1230.
90 H. Cheng, N. Yang, G. Liu, Y. Ge, J. Huang, Q. Yun, Y. Du, C.-J. Sun, B. Chen, J. Liu and H. Zhang, *Adv. Mater.*, 2020, **32**, 1902964.
91 Y. Duan, Y. Wang, W. Zhang, C. Ban, Y. Feng, X. Tao, A. Li, K. Wang, X. Zhang, X. Han, W. Fan, B. Zhang, H. Zou, L. Gan, G. Han and X. Zhou, *Adv. Mater.*, 2024, **36**, 2404900.
92 X. Tian, R. Liu, W. Wang, Q. Yang, Z. Huang, Y. Yang, J. Han, T. Dong, Y. Du, J. Lai, H. Li and L. Wang, *Adv. Mater.*, 2025, **37**, e06068.
93 F. Heck, L. Grunenberg, N. Schnabel, A. Heilmaier, T. Sottmann, L. Yao and B. V. Lotsch, *Adv. Mater.*, 2025, **37**, 2415882.
94 X. Wu, X. Tian, W. Zhang, X. Peng, S. Zhou, P. J. S. Buenconsejo, Y. Li, S. Xiao, J. Tao, M. Zhang and H. Yuan, *Angew. Chem., Int. Ed.*, 2024, **63**, e202410411.
95 J. Huang, Y. Shi, J. Xu, J. Zheng, F. Zhu, X. Liu and G. Ouyang, *Adv. Funct. Mater.*, 2022, **32**, 2203171.
96 M. R. Benzigar, S. Joseph, H. Ilbeygi, D.-H. Park, S. Sarkar, G. Chandra, S. Umapathy, S. Srinivasan, S. N. Talapaneni and A. Vinu, *Angew. Chem., Int. Ed.*, 2018, **57**, 569–573.
97 S. Wan, N. Musielak, A. G. Oliver and A. Jaffe, *Angew. Chem., Int. Ed.*, 2023, **62**, e202314523.
98 N. He, Y. Zou, C. Chen, M. Tan, Y. Zhang, X. Li, Z. Jia, J. Zhang, H. Long, H. Peng, K. Yu, B. Jiang, Z. Han, N. Liu, Y. Li and L. Ma, *Nat. Commun.*, 2024, **15**, 3896.
99 J. Zhang, R. Dai, J. Yang, Y. Liu, J. Yu, L. Tan and Y. Chen, *Energy Environ. Sci.*, 2025, **18**, 3235–3247.
100 W. Shao, J. H. Kim, J. Simon, Z. Nian, S.-D. Baek, Y. Lu, C. B. Fruhling, H. Yang, K. Wang, J. Y. Park, L. Huang, Y. Yu, A. Boltasseva, B. M. Savoie, V. M. Shalaev and L. Dou, *Science*, 2024, **384**, 1000–1006.
101 Q. Li, Z. Dai, J. Wu, W. Liu, T. Di, R. Jiang, X. Zheng, W. Wang, X. Ji, P. Li, Z. Xu, X. Qu, Z. Xu and J. Zhou, *Adv. Energy Mater.*, 2020, **10**, 1903750.
102 J. Zhong, S. Huang, Y. Cao, K. Pei, D. Zhang, X. Lin, H. Long, H. Chen, Y. Liang, X. Zhou and S. Zhang, *Adv. Funct. Mater.*, 2025, **36**, e14143.
103 Z. Lv, M. Liu, Y. Yang, T. Chen, W. Yang, Y. Wang, Z. Zhao, K. Lan, T. Zhao, Q. Li, X. Li and D. Zhao, *J. Am. Chem. Soc.*, 2025, **147**, 14585–14594.
104 D. Chen and S. Mu, *Adv. Mater.*, 2024, **36**, 2408285.
105 D. Kim, Y. Kang, H. Kim, S. Oh, S. Jang, M. Lee, Z. F. Lee, G.-D. Sim and K. T. Lee, *Adv. Mater.*, 2025, **43**, 2506905.
106 H. Yu, S. Jang, D. Lee, G. Youn and K. T. Lee, *Adv. Mater.*, 2025, **37**, 2500183.
107 B. Zhou, J. Wang, L. Guo, H. Li, W. Xiao, G. Xu, D. Chen, C. Li, Y. Du, H. Ding, Y. Zhang, Z. Wu and L. Wang, *Adv. Energy Mater.*, 2024, **14**, 2402372.
108 X. Wu, Z. Wang, D. Zhang, Y. Qin, M. Wang, Y. Han, T. Zhan, B. Yang, S. Li, J. Lai and L. Wang, *Nat. Commun.*, 2021, **12**, 4018.
109 J. Huang, X. Xu, Y. Yan, Y. Zheng, Y. Yao, Z. Li, Y. Yan, K. N. Hui, J. Zou and M. Liu, *Adv. Energy Mater.*, 2025, **15**, 2500360.
110 M. Wen, N. Sun, L. Jiao, S.-Q. Zang and H.-L. Jiang, *Angew. Chem., Int. Ed.*, 2024, **63**, e202318338.
111 H. Ahn, R. A. Senthil, S. Jung, A. Kumar, M. Ubaidullah and M. Y. Choi, *eScience*, 2025, **5**, 100408.
112 R. Zhang, J. Chen, Y. Huang, J. Tang, R. Zhao, Y. Liu, L. Lei, D. Wang, L. Li and Z. Liu, *Adv. Funct. Mater.*, 2025, **35**, 2502205.
113 H. Yuan, D. Jiang, Z. Li, X. Liu, Z. Tang, X. Zhang, L. Zhao, M. Huang, H. Liu, K. Song and W. Zhou, *Adv. Mater.*, 2024, **36**, 2305375.
114 Y. Xie, S. Xu, A. C. Meng, B. Zheng, Z. Chen, J. M. Tour and J. Lin, *Energy Environ. Sci.*, 2024, **17**, 8670–8682.
115 L. Wan, H. Song, X. Chen, Y. Zhang, Q. Yue, P. Pan, J. Su, A. A. Elzatahry and Y. Deng, *Adv. Mater.*, 2018, **30**, 1707515.
116 W. Pan, C. Liang, Y. Sui, J. Wang, P. Liu, P. Zou, Z. Guo, F. Wang, X. Ren and C. Yang, *Adv. Funct. Mater.*, 2022, **32**, 2204166.
117 Z. Wang, S. Yuan, H. Tian, T. Zang, J. Li, J. Liu, G. Li, J. Wang, T. Liu and Q. Wang, *Appl. Catal., B*, 2024, **343**, 123579.

118 S. Ma, K. Wang, M. Rafique, J. Han, Q. Fu, S. Jiang, X. Wang, T. Yao, P. Xu and B. Song, *Angew. Chem., Int. Ed.*, 2024, **63**, e202412821.

119 Y. Tong, E. Bladt, M. F. Aygüler, A. Manzi, K. Z. Milowska, V. A. Hintermayr, P. Docampo, S. Bals, A. S. Urban, L. Polavarapu and J. Feldmann, *Angew. Chem., Int. Ed.*, 2016, **55**, 13887–13892.

120 L. Zhang, Y. Zhang, X. Li, D. Han, W. Zhai and J. Wang, *Adv. Sci.*, 2025, **12**, 2414438.

121 Z. Li, H. Zhang, D. Wang, C. Gao, M. Sun, Z. Wu and Q. He, *Angew. Chem., Int. Ed.*, 2020, **59**, 19884–19888.

122 M. Kløve, S. Sommer, B. B. Iversen, B. Hammer and W. Dononelli, *Adv. Mater.*, 2023, **35**, 2208220.

123 E. Vargo, J. C. Dahl, K. M. Evans, T. Khan, P. Alivisatos and T. Xu, *Adv. Mater.*, 2022, **34**, 2203168.

124 Z. Ghahramani, *Nature*, 2015, **521**, 452–459.

125 M. I. Jordan and T. M. Mitchell, *Science*, 2015, **349**, 255–260.

126 F. Wang, L. Xie, N. Sun, T. Zhi, M. Zhang, Y. Liu, Z. Luo, L. Yi, Q. Zhao and L. Wang, *Nano-Micro Lett.*, 2023, **16**, 32.

127 Y. Li, S. Kumar, G. Yang, J. Lu, Y. Yao, K. Kang and Z. W. Seh, *Science*, 2025, **389**, eadl5482.

128 S. Zhang, L. Zhang and Z.-S. Wu, *ACS Nano*, 2024, **18**, 24617–24621.

129 S. Mitchell, R. Qin, N. Zheng and J. Pérez-Ramírez, *Nat. Nanotechnol.*, 2020, **16**, 129–139.